# Contrast and complexity in the low temperature kinetics of CN(v=1) with $O_2$ and NO: Simultaneous kinetics and ringdown in a uniform supersonic flow

Shameemah Thawoos[a], Gregory E. Hall[b], Nicolas Suas-David[c], and Arthur G. Suits[a*]

[a] *Department of Chemistry, University of Missouri, Columbia, MO 65211, USA*

[b] *Chemistry Division, Brookhaven National Laboratory, Upton, NY 11973, USA*

[c] *Univ Rennes, CNRS, Institut de Physique de Rennes - UMR 6251, F-35000 Rennes, France*

*suitsa@missouri.edu

## Abstract

Bimolecular rate coefficients were determined for the reaction CN(v=1) + NO and $O_2$ using continuous wave cavity ringdown spectroscopy in a uniform supersonic flow (UF-CRDS). The well-matched timescales for ringdown and reaction under pseudo first-order conditions allow for the use of the SKaR method (simultaneous kinetics and ringdown) in which the full kinetic trace is obtained on each ringdown. The reactions offer an interesting contrast in that the CN(v=1) + NO system is nonreactive and proceeds by complex-mediated vibrational relaxation, while the CN(v=1) + $O_2$ reaction is primarily reactive. The measured rate coefficients at 70 K are (2.49 ± 0.08) × $10^{-11}$ $cm^3$ $molecule^{-1}$ $s^{-1}$, respectively, for the reaction of $O_2$ and (10.49 ± 0.22) × $10^{-11}$ $cm^3$ $molecule^{-1}$ $s^{-1}$ for reaction with NO. The rate for reaction with $O_2$ is a factor two lower than previously reported for v=0 in the same temperature range, a surprising result, while that for NO is consistent with extrapolation of previous high temperature measurements to 70 K. The latter is also discussed in light of theoretical calculations and measurements of the rate constants for the association reaction in the high-pressure limit. The measurements are complicated by the presence of a metastable population of high-J CN formed by photolysis of the precursor BrCN, and a kinetic model is developed to treat the competing relaxation and reaction. It is particularly problematic for reactions at low temperature where the rotational relaxation and reaction have similar rates, precluding a reliable determination of the rate coefficients at 30 K. Also presented are important modifications to the data acquisition and control for the instrument that have yielded considerably enhanced stability and throughput.

## 1 Introduction

The study of elementary reaction kinetics at very low temperatures contributes significantly to understanding and modeling the chemistry of planets, moons, and interstellar clouds. Experimental determination of the rates of reactions at very low temperatures is a challenge due to condensation on the walls of the reactor. This impediment has been overcome with the introduction of the CRESU method, a French acronym that translates to "*reaction kinetics in uniform supersonic flows*"[1]. The CRESU method employs a Laval nozzle, an axisymmetric convergent divergent nozzle that produces a uniform supersonic flow which act as a wall-less reactor[2-4]. Since the inception of the CRESU method it has undergone many developmental advances which addressed its limitations, the most serious of which has been the huge pumping capacity required as well as the large consumption of gases. The widely used solution to this has been using a pulsed Laval flow, first introduced by Atkinson and Smith.[5] Since then, pulsed Laval flows have been adopted by many other groups, including ours[6-8]. Although the CRESU method has been coupled with various detections methods, the overwhelming majority of studies reported using laser-induced fluorescence (LIF). In this report we will focus on our new experiment where we have coupled a pulsed uniform flow system with a near infrared continuous wave cavity ringdown spectrometer (*cw*-CRDS)[8], a combination we term UF-CRDS. CRDS is a highly sensitive absorption technique which is also largely immune to fluctuations in the source intensity and is a promising alternative compared to the LIF method which is inherently limited to a few target species. Given the long ringdown times (several hundred microseconds) and the corresponding well-matched hydrodynamic times of the pulsed Laval flow of the UF-CRDS, we have been able to measure the complete kinetics in each ringdown decay, an approach termed SKaR (Simultaneous Kinetics and Ringdown)[9]. We first demonstrated this for reaction of CN(v=1) with propene[8], and more recently determined the low temperature reaction rate coefficients for CN (v=1) reaction with butadiene isomers[10].

Reactions of CN are of considerable importance in understanding formation of nitrogen rich compounds in many different environments including combustion, interstellar clouds, and the atmospheres of planets and their moons. Therefore, there is a great interest in studying reactivity of CN with wide varieties of co-reactants in varying reaction conditions, with low temperature measurements particularly important for astrochemistry. CRESU[1, 3, 11-12] coupled with LIF has been applied to many studies of the reactions of CN with various co-reactants including small molecules such as $O_2$[13-14] $H_2$,[14] small hydrocarbons[15-16], NOx[17-18], amines[19], and many more[20-22]. Typical LIF detection of CN, where the (0,0) band of the $B^2\Sigma$-$X^2\Sigma$ transition is excited at ~387 nm with fluorescence is detected on the (0,1) emission at 420 nm. This created a path to

extensive investigation of these reactions at temperatures down to 5.8 K[23-24]. However, the literature in low temperature kinetics have been primarily dominated by CN(v=0) even though there is evidence of the presence of vibrationally excited species in many reaction environments and interesting issues are raised in comparing the rates of the vibrationally excited CN with ground state CN. It is important to understand the role of the vibrationally excited reactants as the overall reaction rate either can be controlled by reactive processes, non-reactive relaxation, or significant contributions from both. Our ability to probe CN(v=1) in the UF-CRDS system permits us to explore the reactive and non-reactive relaxation rates of vibrationally excited CN. In this report we present two systems with contrasting behavior, reaction of CN(v=1) with $O_2$ and NO.

There are many studies reported for the reaction of ground state CN and $O_2$ at temperatures ranging as high as 4000 K to as low as 13 K, and theoretical studies to support these measurements[4, 25-30]. It is considered to be one of the classic radical-radical reactions and the first neutral-neutral reactions studied using the CRESU apparatus in Rennes[25]. The reaction between CN and $O_2$ can lead to three different exothermic product channels as sketched in the schematic potential energy surface in figure 1(a) [28, 31-32].

$$CN + O_2 \longrightarrow NCO + O \qquad (1)$$

$$CO + NO \qquad (2)$$

$$N + CO_2 \qquad (3)$$

Among the three pathways, the dominant reaction channel is that forming products NCO and O (1) while the channel leading to N and $CO_2$ (3) is either minor or completely unobserved. The CN + $O_2$ reaction can take place on potential energy surfaces of doublet or quartet spin multiplicity with the latter considered non-reactive, giving an electronic degeneracy factor for the rate of 1/3. On the doublet surface, the reactants can approach without a barrier to form a bent NCOO complex bound by ~35-40 kcal/mol, then to products. O-O bond fission then leads to dominant products NCO+O[29, 33-34]. Although there is a substantial barrier involving a four-center transition state to NO + CO, Jackson and coworkers[32] instead proposed intramolecular abstraction of N by an O atom, anticipating the roaming mechanism several years before it was clearly identified in formaldehyde photodissociation[35]. This raises the question of the barrier to the O-O bond fission in the complex: the existence of a barrier would likely preclude the roaming pathway suggested by Jackson, but recent measurements clearly document the presence of this channel. There is only one direct measurement of the kinetics of the O + NCO reaction, and that found a fast room temperature rate with a negative temperature dependence consistent with a barrierless process. Vallance

and coworkers have reported a G2-level investigation of the stationary points and found a modest barrier to NCO + O elimination[34]. However, it seems likely that a single reference treatment may not be suitable to identify this TS, and to our knowledge, no multi-reference treatments of that TS have been reported. Davis and coworkers reported crossed-beam measurements of the CN + $O_2$ reaction monitoring the O atom product using their O atom variant of the Rydberg time of flight method. They found a nearly isotropic distribution and a translational energy distribution that peaked at ~ 5 kcal/mol. This would be consistent with a modest exit barrier, but dynamical effects may also be responsible. Indeed, Davis and coworkers suggest the possibility that the low translational energy component may be preferentially depleted by the roaming reaction. Although not definitive, it seems the NCO-O fission is likely barrierless and O atom roaming can give NO + CO as suggested by Jackson et al.[32]

Over the wide range of temperature, the reaction has been studied experimentally, the rate is nearly independent of temperature from 4000 K down to 700 K, but the rate increases when the temperature is reduced below 700 K down to 13 K[4, 17, 28-30, 36]. Moreover, there are few experiments that have studied the influence of the vibrational excitation of CN on the rate of reaction[17, 37] and findings are inconsistent. This will have considerable bearing on our measurements and will be addressed more fully in the Discussion below.

Relevant stationary points on the PES for the CN + NO reaction are given in figure 1b. This reaction involves the NCNO intermediate which is well-characterized, in contrast to NCOO. The fate of association of CN and NO can be given by the following[38].

$$CN(v) + NO \longrightarrow N_2 + CO \quad (4)$$

$$CN(v) + NO + M \longrightarrow NCNO + M \quad (5)$$

$$CN(v) + NO(v'=0) \longrightarrow CN(v-1) + NO(v'=1) \quad (6)$$

LIF based investigations of the reactions of CN (v=0) and (v=1) at room temperature and above suggest the reaction of (v=1) with NO predominantly occurs via non-reactive vibrational relaxation process (6). This rate is much faster than either pathway leading to products though they are highly exothermic in nature (-635.8 kJ/mole and -204.3 kJ/mole for reaction (4) and (5) respectively)[18]. The increased rate due to vibrational relaxation can be explained by the energy gap law. Experimental results at low temperature and supporting theoretical calculations of CN + NO suggest the reaction occurs predominantly via a transient complex formation yielding NCNO, though the less stable CNNO isomer and the triplet intermediate are also believed to participate [18, 39]. The vibrationally excited complex then re-dissociates through a non-reactive relaxation

process[40]. The vibrational quenching is faster when the energy gap is smaller and the energy gap between the CN and NO for *v*=1 is 165 $cm^{-1}$. According to literature, the rate of loss of CN above room temperature for v=1 is significantly faster in the presence of NO compared to pressure dependent rates of v=0[17-18]. However, the significant enhancement in the rate of loss of CN (v=1) vs (v=0) can be attributed to formation and dissociation of the NCNO complex though a barrierless pathway analogous to the $O_2$ case above but without a reactive component.

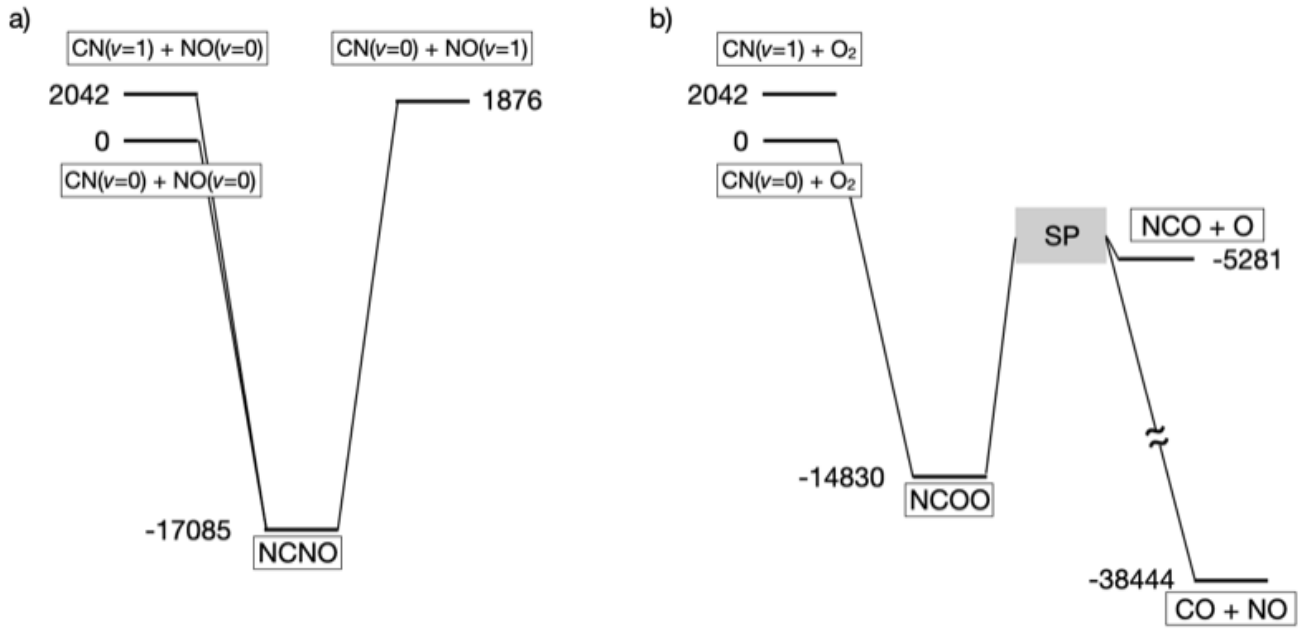


*Figure 1. Relevant stationary points on the potential energy surface for CN + NO (a) and CN + $O_2$ (b), energies in $cm^{-1}$. NCNO energy from reference[41], NCOO energy from G2(MP2) calculations in reference [34]. NCO + O and CO + NO exoergicities from Active Thermochemistry Tables[42]. SP: saddle point, see text.*

## 2 Experimental Methods

The experiments reported here are carried out using the newly developed instrument UF-CRDS. A detailed account of the instrumentation and the design is given in a previous publication[8]. There has since been considerable modification to the data acquisition to improve the throughput of the instrument and it will be discussed here.

### *2.1 Instrumentation*

The pulsed Laval flow and the *cw*-CRD spectrometer is housed in a stainless-steel chamber. The pulsed Laval flow system is achieved using a home built high-throughput piezoelectric stack[43] valve and a Laval nozzle.

Laval nozzles are fabricated in-house using a filament-based commercial 3D printer (Ultimaker3-Extended). We use PLA (poly lactic acid) filaments to print the nozzles, as we have found the PLA printed nozzles to be robust and able to withstand the experimental conditions, including exposure to the excimer laser pulses. The 70 K nozzle presented here is one such 3D printed nozzle, used without any post-treatment of the print. A second nozzle, originally designed for a nominal 25 K flow of Ar, was also used in the present experiments with Ne gas to produce a uniform 30 K flow. The piezoelectric stack valve fills up a reservoir of approximately 20 $cm^3$ and the gas is expanded through the Laval nozzle into a vacuum chamber producing a collimated uniform flow. The average flow rate into the reservoir is controlled by one or multiple flow controllers (Alicat Scientific - MCS series) upstream from the pulsed stack valve. The Laval nozzle and the piezoelectric stack valve assembly are mounted on motorized actuators which enables movement horizontally along the flow direction, and vertically inside the chamber.

The ultra-pure, research grade carrier gases Ne (NOVA gas), $N_2$, $O_2$ (AirGas), NO (Praxair) and cyanogen bromide (BrCN) were used as purchased without any further treatment. Vibrationally excited CN was produced via photolysis of BrCN using a 248 nm excimer laser aligned along the nozzle axis and counter propagated to the flow. The laser fluence at the exit of the nozzle was at approximately 100 mJ $cm^{-2}$ and the BrCN density in the flow adjusted such that the maximum estimated CN produced was $3 \times 10^{11}$ molecule $cm^{-3}$. The overlap of the cw-CRDS probe and the photolysis volume was optimized via a periscope, where

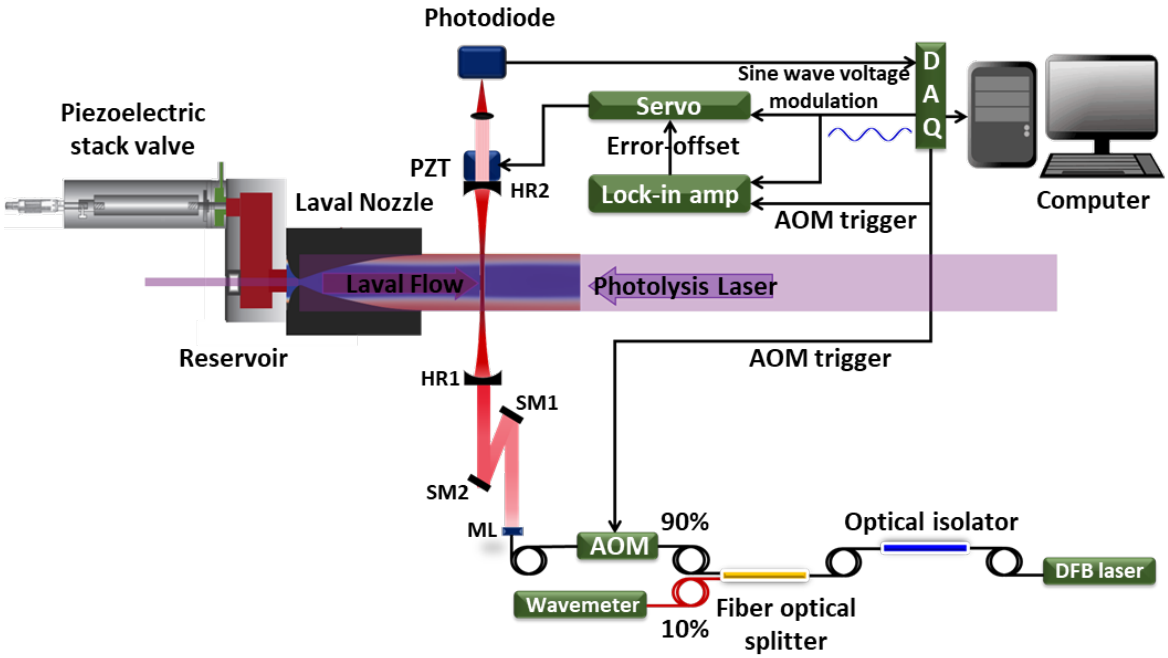


*Figure 2. Schematic overview of the key components of the UF-CRDS apparatus.*

the laser beam is rotated, and the elongated side of the beam is aligned horizontally. In addition, the beam was loosely focused using a cylindrical lens (2 m focal length).

To probe vibrationally excited CN radicals the CRD spectrometer is equipped with a distributed feedback (DFB) diode laser centered around 7070 $cm^{-1}$, with a tuning range adequate to cover the low-J lines of the $^{r}R_1$ branch of the CN $A^2\Pi$-$X^2\Sigma^+$ (0-1) transition. The CRD spectrometer is composed of two plano-concave mirrors (HR1 and HR2) with 1 m radius of curvature, which are set up perpendicular to the pulsed Laval flow. The high-reflectivity plano-concave mirrors are separated by 80 cm and mounted on the chamber via bellows which isolate the cavity mirrors from vibrations of the main chamber. The cavity mirrors are constantly flushed with a flow of nitrogen gas (typically near 600 sccm) which also act as a "slip gas," maintaining the background chamber pressure required to obtain well-collimated flow conditions. A fiber splitter directs about 10% of the laser output to a wavemeter, while most of the laser output enters a fiber coupled acousto-optical modulator (AOM). The deflected output of the AOM is coupled out of the fiber and injected into the cavity via two steering mirrors (SM1 and SM2) and a mode matching lens (ML). The injection of light into the cavity is interrupted by the triggered amplitude switching of the RF driver for the AOM. The output cavity mirror is mounted on a piezoelectric transducer (PZT) which allows the modulation of the cavity length to match cavity resonances to the narrow laser line width. The transmitted light from the output cavity mirror is focused onto a photodiode and this monitors the ringdown events. An overview of the key features of the experimental setup is shown in figure 2.

The gas mixture supplied to the pulsed Laval nozzle is the combined outputs of three Alicat MCS type flow controllers with full-scale ranges of 2000, 1000 and 10 sccm (standard cubic centimeters per minute). The first provides pure carrier gas. The second provides a dilute mixture of BrCN vapor entrained in a flow of the same carrier gas, with the BrCN content adjusted with flow rate and the temperature of a metal "bubbler" containing finely ground BrCN powder. The third flow controller provides adjustable increments of the co-reactant, $O_2$ or NO, typically pre-mixed in a 25-30% dilution with the carrier gas.

### *2.2 Timing and Data Acquisition*

Since our initial report on the use of cw-CRDS to measure kinetics in the uniform flow machine,[8] the timing scheme and data acquisition code has been significantly revised to improve stability and throughput. A servo feedback loop was implemented to keep the cavity modulation cycle centered on one transmission fringe,

eliminating the slow drift of fringe timing relative to a 50 Hz cavity modulation, even during short scans across Doppler profiles. With this stabilization, the entire pattern of timing signals can be generated in hardware, (National Instruments 6351) without depending on real-time software tests or loops. Figure 3 illustrates this timing sequence.

A 50 Hz sinusoidal cavity modulation signal with an adjustable, phase-synchronized timing pulse is generated by continuously retriggered analog outputs from a FIFO buffer in the DAQ multifunction board. The synchronization pulse triggers a counter that provides a pulsed nozzle trigger of adjustable delay and duration at a divide-by-N sub-harmonic of the modulation frequency. The delay is chosen to precede the next anticipated cavity fringe by typically 3-4 ms, the time it takes from the nozzle trigger until uniform flow conditions are established at the downstream position of the CRD beam. The DC bias applied to the cavity piezo transducer is controlled by a servo feedback amplifier (New Focus LB 1005) with an error signal derived from a lock-in amplifier referenced to the 50 Hz modulation signal and processing the detected fringe timing signals. When locked, the cavity is modulated with an amplitude somewhat less than one free spectral range, with transmission fringes occurring on average at the plus and minus zero crossings of the modulation cycle, i.e., 100 fringes per second. The photodiode monitoring the transmission fringes and the ringdown signals generates a threshold trigger event to trigger the AOM switching that initiates the ringdown, as well as a clock burst for the 1 MHz acquisition of an analog ringdown signal waveform, and the trigger to start a 25 μs delay before generating an external trigger for the excimer photolysis laser, having been armed at the time of the last nozzle trigger. The timing jitter between a given pulsed nozzle trigger event and the next cavity transmission fringe is typically distributed with a standard deviation of around 1 ms around the chosen delay time. The trigger threshold for capturing a ringdown signal is typically set to capture 80-90% of the fringes, so that in addition to the ~1 ms timing indeterminacy for the “right” fringe, the next fringe after the nozzle trigger may be below the triggering threshold. In this case, a subsequent fringe, occurring at a small integer multiple of 10 ms later than the anticipated time will initiate the ringdown acquisition and laser trigger at a time too late to allow interrogation of the gas pulse, which lasts less than 5 ms. To sort the recorded ringdown waveforms according to the time within the gas pulse and to identify those ringdown signals that are not synchronized with the gas pulse, a timer in the DAQ multifunction board is started with the nozzle trigger and stopped with the photolysis laser trigger, derived from the photodiode threshold detection. All these timing tasks are defined as asynchronous processes, running autonomously on the DAQ multifunction board.

The data acquisition is interrupt driven (referred to as dynamic events in LabView), reading a new timer value when the data is ready (at the repetition rate of the nozzle and photolysis laser) and reading a new ringdown waveform whenever a complete ringdown data buffer is ready to read, (at approximately 100 Hz).

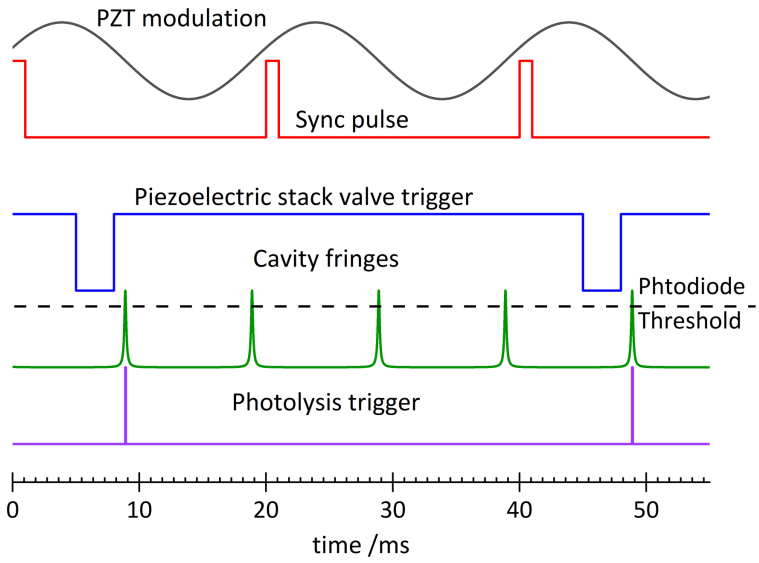


*Figure 3. Timing signals used in UF-CRDS. Illustration shows Piezo Stack trigger at 25 Hz (divide-by-2) for graphical clarity; actual operation at 5 Hz or 10 Hz (divide by 10 or 5) is generally dictated by limitations of pumping speed. Cavity fringes are shown without typical fluctuations in timing and amplitude.*

We use a data queue to combine each ringdown waveform and its system timestamp with a copy of the most recently recorded timer value and its timestamp and add this cluster of data as the next element in the data queue. In this way, the ringdown data associated with the gas pulse and photolysis laser is evident as the first one with a new value of the timer reading, which in turn can be used to accumulate ringdown data in bins according to their time relative to the start of the gas pulse. The ringdown events not associated with a gas pulse can be combined to give an average background ringdown signal for reference. All the time-critical data acquisition steps are performed in an event-driven producer loop that adds records to the data queue, while all diagnostic, plotting, binning, and storage tasks can be done in an asynchronous queue-consuming loop, tolerant to processing lags or occasional CPU-heavy tasks without losing or mislabeling data. At a fixed probe wavelength, signal acquisition proceeds by retrieving the oldest element of the data queue and deciding if it is the first record with a new timer value. If so, the timer value is used to choose which 200 µs wide time bin to accumulate the ringdown signal in, incrementing the number of hits in the appropriate time bin and updating the sum of ring down signals in that bin. All other ringdown signals are instead accumulated in a running average of background ringdown curves. Once a desired number of

averages has been accumulated, a file is saved with the time-sorted ringdown events associated with a gas pulse and photolysis laser, the background average ringdown signal, and the rest of the relevant experimental parameters under computer control. A scanning mode has also been implemented, which repeats this process at each step of the probe laser and saves a catenated file of similar contents at each dwell frequency of the scan.

## 3 Results

### *3.1 Flow Characterization*

Measurements presented here were performed with two different nozzles to access nominal temperatures of 70 K in $N_2$ and 30 K in Ne. The nozzles have been characterized with transverse and longitudinal scans of impact pressure with pure gas expansions in the movable nozzle assembly and a fixed Pitot sensor, as described in earlier work [8]. Key properties of the flow from these nozzles are summarized in Table 1. The overall duration of the gas pulses is controlled by a 3 ms opening pulse applied to the stack valve supplying gas to the reservoir and the establishment of steady flow conditions before the gas supply is stopped. A central 0.5-1 ms portion of each gas pulse was typically found to have effectively identical spectroscopic and kinetic diagnostics, as the relative timing of the triggering of the stack valve and the laser-initiated photochemistry was varied. The observation time available for kinetic measurements was determined by the downstream position of the CRD detection relative to the movable nozzle, along with the flow velocity. The present measurements were performed 150 mm downstream from the nozzle exit, providing approximately overall 200 μs and 220 μs windows for kinetic observation in the 30 K Ne and 70 K $N_2$ flows, respectively, before the photoproducts formed in the throat of the nozzle arrive at the CRD probe region and spoil the uniformity of the reactant column passing through the probe region.

*Table 1. Summary of flow conditions used.*

| Carrier gas | Design temperature/ K | Measured temperature / K | | Mach number | Peak flow density/ molecule $cm^{-3}$ | flow velocity/ $ms^{-1}$ | Isentropic core diameter‡/ mm |
|---|---|---|---|---|---|---|---|
| | | Pitot | CN rotational Boltzmann plot | | | | |
| $N_2$ | 70 | 71.3 ± 2.8 | 75.1 ± 2.7 | 4.0 ± 0.1 | $5.5 \times 10^{16}$ | 690 | 20 |
| Neon | 25 (Ar)* | 30.6 ± 1.2 | 33.7 ± 1.2 | 5.1 ± 0.1 | $4.5 \times 10^{16}$ | 740 | 15 |

** The nozzle used here is originally designed for Ar gas producing a flow of 25 K.*

‡ *The flow remains laminar up to about 200 mm and typically the experiments are conducted at 150 mm from the exit of the nozzle.*

In addition to the flow temperatures calculated from the Pitot impact pressure measurements, the rotational temperature of the CN(v=1) can be measured from relative intensities of multiple low-J lines in

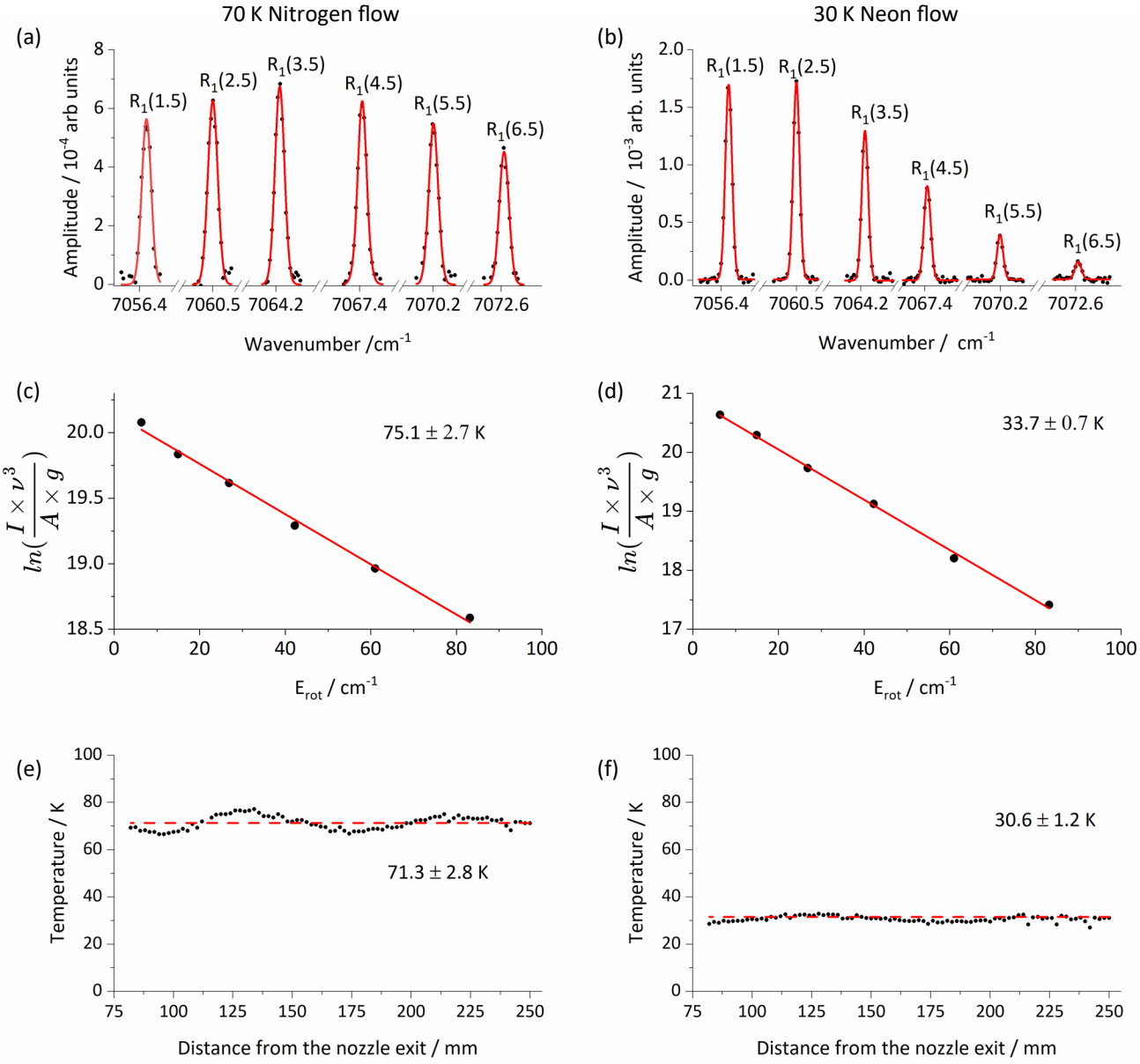


*Figure 4. Laval flow characterization. Rotational lines of CN $A^2\Pi$-$X^2\Sigma^+$ (0-1) $^rR_1$ branch spectrum (a and b) and the Boltzmann plot derived from the spectra 102 µs after the photolysis (c and d). The temperature calculated from the impact pressure measurements along the axis of the flow (e and f). Left panels are from the 70 K Nitrogen flow and right is from 30 K Neon flow.*

the CRD spectrum of the CN photoproducts from 248 nm photolysis of BrCN. Figures 4 a and b illustrate a Doppler scan using 0.002 $cm^{-1}$ steps across the low-J lines of the $^rR_1$ branch of the *A-X* (0-1) band. The intensities at each dwell frequency of the spectrum were obtained by computing the local decay rate of the ringdown signal in a 5 μs gate delayed 100 μs from the photolysis laser, relative to the background ringdown rate (in the absence of the gas pulse and photolysis laser). Figure 4 c and d are Boltzmann plots of the intensities, corrected for the degeneracy $g=2J+1$, the Einstein A factor[44] and the transition frequency $\nu$, relative to the rotational energy of the detected CN (v=1) states. The slopes yield a rotational temperature in good agreement with the gas dynamic temperature computed from the Pitot measurement of impact pressure as a function of distance downstream from the nozzle on the centerline of the flow, depicted in figures 4 e and f. All these experiments were carried out in both Nitrogen and Neon flow, as demonstrated in the left and right panels of figure 4, respectively. In principle, the Doppler-broadened line widths give yet another probe of the translational temperature in the flow. The apparent temperatures deduced from Gaussian fits to the lines are, however, systematically warmer than the temperatures based on the pitot measurements or the rotational distribution ns, typically by 30-50 K, rendering the line widths a less useful diagnostic than we had hoped for. The discrepancies may have contributions from warmer CN radicals in the boundary layer, deviations from perfect orthogonal probing relative to the flow direction, imperfect collimation of the flow, and fluctuations in the probe laser frequency during signal averaging.

### *3.2 Production and Thermalization of CN (v=1)*

An ideal scenario for the measurement of thermal rate constants for the reactions of vibrationally excited CN by monitoring rotationally resolved spectra would be to have a prompt photolytic source of rotationally thermalized but vibrationally excited CN, whose disappearance rate can be measured as a function of added co-reactant, using any convenient rotational transition. Efficient rotational energy transfer collisions with the thermal bath gas can often approximate this ideal situation in spite of nascent non-thermal state distributions produced in photolysis, as long as the vibrational relaxation and bimolecular reaction of interest remain significantly slower than the rotational thermalization rates. Cyanogen halides are convenient photolytic sources of CN radicals commonly used for kinetic studies and their ultraviolet photodissociation dynamics have been explored extensively[45-52]. Photodissociation of BrCN at 248 nm is a good source of vibrationally excited CN (v=1) although the nascent rotational distribution is highly excited, with a significant fraction at very high rotational levels [49-50]. The decreasing efficiency of rotational energy collisions for high angular momentum states,[53-54] where the rotational energy gaps exceed the typical

collision energies, can result in an evolving bimodal rotational state distribution that includes a growing thermal component and a more persistent, highly excited component.[47, 51-52] Our observations of a growing thermal component are consistent with these previous reports.

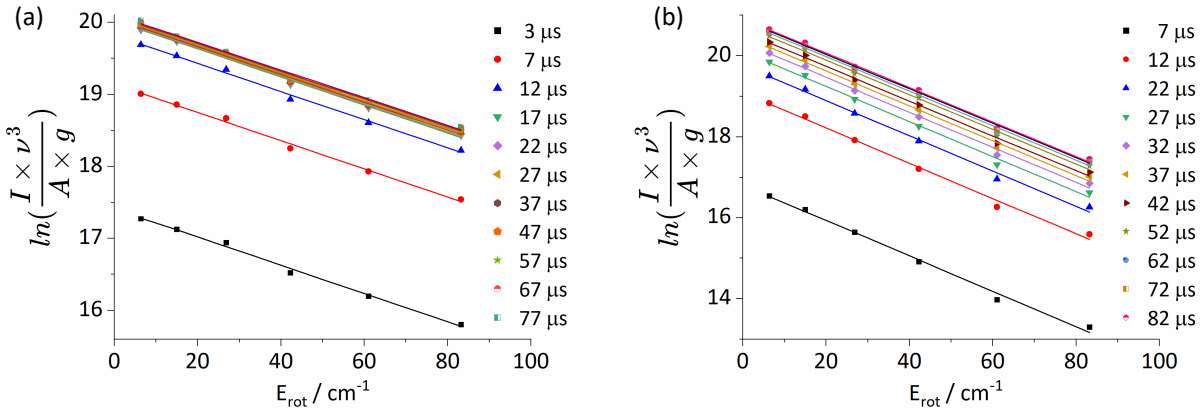


*Figure 5. Rotational distribution for low J levels of the CN $A^2\Pi$-$X^2\Sigma^+$ (0-1) $^rR_1$ branch in (a) 70 K and (b) 30 K flow as a function of time after photolysis.*

At high dilution of reagents in an inert collisional environment, the rotational thermalization can still be fast enough to permit separable timescales of thermalization and reaction, but we have found that at the lower temperatures accessible in this study, the continued growth of thermalized CN (v=1) needs to be considered in the interpretation of the kinetics. Figure 5 illustrates the rotational distribution of CN (v=1) in the 70 K $N_2$ flow and the 30 K Ne flow as a function of time after photolysis. Even at the earliest times, up to 3 µs after photolysis, the relative populations of the observed low-J states are distributed according to the flow temperature. The total population of these thermal sub-populations, however, grows from a near-zero initial value to within 1/e of the maximum at times about 10 µs at 70 K and 50 µs at 30 K, as shown by the vertical displacement with time of near-parallel lines in the Boltzmann plots.

### *3.3 Simultaneous Kinetics and Ringdown Data Analysis*

Cavity ringdown measurements depend on a change in the rate of loss of optical intensity inside a low-loss cavity due to the incremental effect of molecular absorption. In the notation of Brown, *et al.*[9] who coined the acronym SkaR for simultaneous kinetics and ringdown, a differential equation depicting the combined effects of cavity loss and absorption is Eq 7.

$$\frac{dI}{I} = -\left(\frac{L_A}{L}\, c\, \alpha + \frac{1}{\tau_0}\right) dt \qquad (7)$$

$L_A/L$ is the fraction of the cavity pathlength containing a sample with absorption coefficient $\alpha = \sigma n$, the product of base-e absorption cross section σ and absorber number density n, $c$ is the speed of light, and $\tau_0$ is the empty cavity ringdown time, limited by the mirror reflectivity. For a static sample, $\alpha$ is constant and the integrated expression leads to the usual CRDS expression for an exponential decay in the presence of a molecular absorption that is faster than the exponential decay of the empty cavity:

$$I(t) = I_0 \exp - \left(\frac{L_A}{L}\, c\, \alpha + \frac{1}{\tau_0}\right). \quad (8)$$

When the molecular absorption is time-dependent, the intensity leaving the cavity will decay non-exponentially, with a general integrated form given by Eq 9:

$$I(t) = I_0\ \exp - \left[\, c\, \sigma\, \frac{L_A}{L} \int_0^t n(t)dt + \frac{1}{\tau_0}\right] \quad (9)$$

This non-exponential signal waveform can be normalized by the background ringdown signal, $I_0\, e^{-t/\tau_0}$, measured in the absence of the gas pulse and photolysis laser, to isolate the kinetics of interest in a ringdown ratio, as advocated by Brown et al.[9]:

$$Ratio(t) = \frac{I(t)}{I_0\, e^{-t/\tau_0}} = \exp - \left[\, c\, \sigma\, \frac{L_A}{L} \int_0^t n(t)dt\right] \quad (10)$$

Several limiting cases can be considered. If $n(t) = n_0$, integration of the constant recovers the usual simple exponential decay seen in stable molecule CRDS:

$$Ratio(t) = \exp - \left(c\, \sigma\, n_0\, \frac{L_A}{L} t\right) \quad (11)$$

If $n(t) = n_0 \exp(-kt)$ , as would occur for an instantaneous formation followed by a first-order decay, the ringdown ratio would follow the form,

$$Ratio(t) = \exp - \left[\, c\, \sigma\, \frac{n_0}{k} \frac{L_A}{L} \left(1 - e^{-kt}\right)\right] \quad (12)$$

That is, the ratio is unity before photolysis, then starts to decrease linearly at the time of photolysis, initially following Eq 11, but then decaying more slowly on the timescale of $1/k$ and approaching a constant value as $n(t)$ approaches zero, and the ringdown rate returns to that of the empty cavity, but with reduced intensity.

A third limiting case is a good description of all the current measurements, where the growth and decay of the absorber follow resolvable rise and fall kinetics, as if from a sequential first-order formation and decay:

$$n(t) = n_{X,0}\,\frac{k_r}{k_r - k_f}\left(e^{-k_f t} - e^{-k_r t}\right) \qquad (13)$$

where $n_{X,0}$ is the initial photolytic yield of some species $X$ which forms the detected absorber with a rising rate $k_r$, while being consumed at rate $k_f$. In this case, the ratio lacks the discontinuous change in slope at the time of photolysis, as would be observed with a prompt photolytic formation of an initial concentration of the detected absorber.

Figure 6 illustrates a typical measurement for which this difference-of-exponentials functional form accurately represents the observed kinetics. The top panel (a) is a semi-log plot of the ringdown signal at the peak of the CN $R_{11}(5.5)$ line in the (0-1) A-X band, plotted along with the averaged background ringdown signal without BrCN photolysis. This particular sample contained $O_2$ at a number density of $1.28 \times 10^{14}$ molecule cm$^{-3}$ in the 70 K flow with a $N_2$ carrier gas in addition to BrCN. The signal $I(t)$ in red is the average of 600 ringdown events, including all those for which the ringdown and photolysis occurred between 3.2 and 4.2 milliseconds after the initial stack trigger, in the central portion of the flow. In this case, about 40% of the recorded ringdown events coincident with a gas pulse and laser photolysis were discarded, as their measured delay times were outside this time window. The background ringdown $I(t) = I_0\, e^{-t/\tau_0}$ in black is an average of about 15000 ringdown events, recorded at approximately

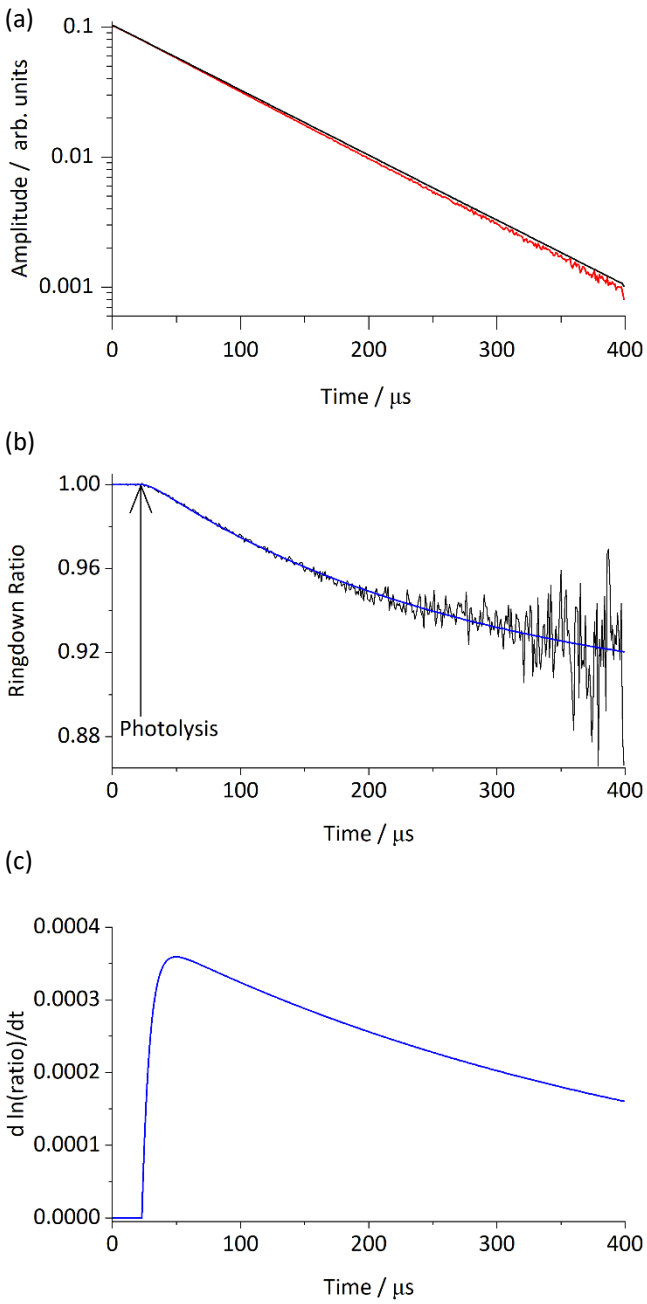


*Figure 6. (a). Ringdown decay profile in the absence (black) and in the presence (red) of changing density of CN(v=1) due to reaction with $O_2$ in the 70 K flow. (b) Signal to background ringdown ratio (black) from (a) and the parameterized fit(blue). (c). Optimized concentration profile Time dependent ratio from the optimized parameterized fit in (b).*

100 Hz during the same time required to get 1000 foreground signals at 5 Hz. The background average includes all those measured ringdown events for which there was no coincident gas pulse. The background ringdown time here is $\tau_0 \approx 95\ \mu s$. The signal to background ratio is plotted on a linear scale in the center panel (b). The initial 23 μs of the ratio, before the photolysis laser fires, has a constant value of 1, as expected, and the ratio decreases thereafter as the CN absorber concentration grows and decays. The noise in the ratio naturally increases at longer times, as both numerator and denominator tend to zero. The smooth curve in figure 6(b) is a least-squares fit of the ratio to the integrated form of the kinetic equation, Eq 10, over the time domain up to 180 μs, in which $n(t)$ is given by the three-parameter function,

$$n(t) = a\left(e^{-k_{fall}t} - e^{-k_{rise}t}\right) \qquad (14)$$

Figure 6(c) shows the best-fit $n(t)$ that optimizes the time-dependent ringdown ratio. When the rise rate is substantially faster than the fall rate, the shape of the ringdown ratio is similar to Eq 12 for a simple first-order decay, and the decay rate could just as well be extracted from a pure decay functional form after neglecting the earliest time portions of the ringdown ratio.

In contrast, figure 7 shows analogous data for a similar density ($1.06 \times 10^{14}$ molecule cm$^{-3}$) of $O_2$ in the 30 K Ne flow. The time to reach the maximum concentration is significantly longer,

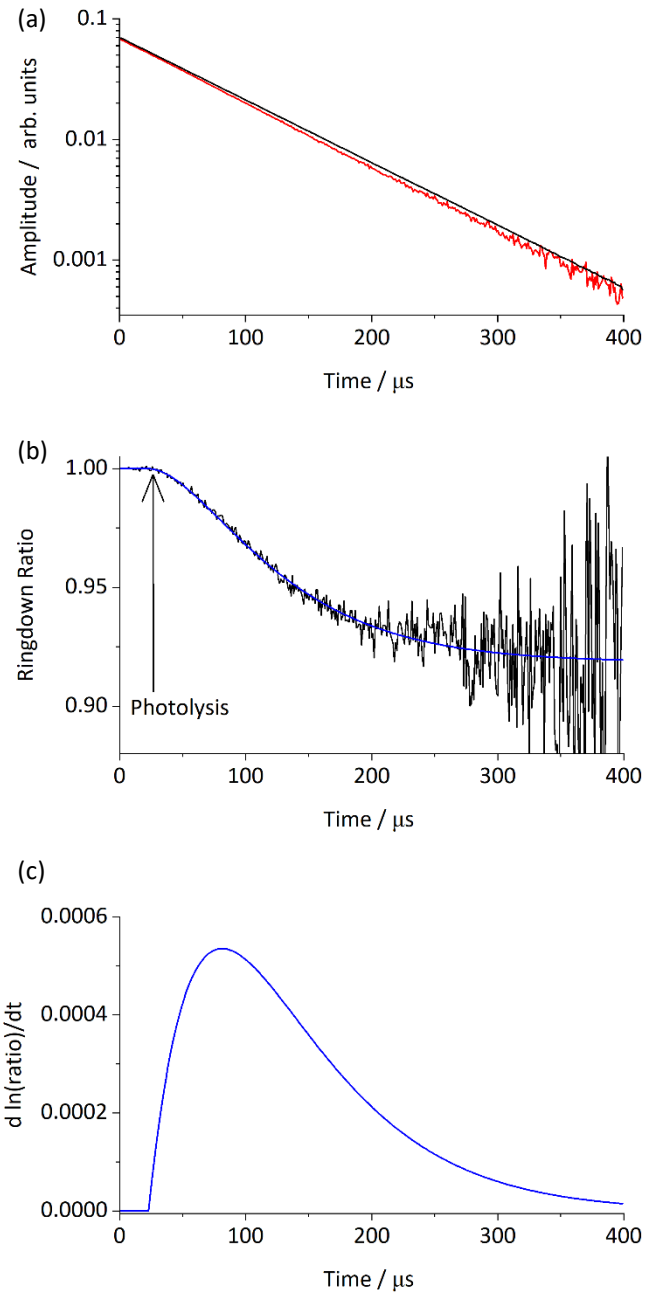


*Figure 7. (a). Ringdown decay profile in the absence (black) and in the presence (red) of changing density of CN(v=1) due to reaction with $O_2$ in the 30 K Ne flow. (b) Signal to background ringdown ratio (black) from (a) and the parameterized fit(blue). (c). Time dependent concentration profile, optimized to produce the fit to the ringdown ratio in (b).*

and the timescales for growth and decay are more similar. The three-parameter functional form Eq 14 remains flexible enough to capture the key features of the measured time-dependent ringdown ratio. The $^rR_1(5.5)$ line near 7070 $cm^{-1}$ used for the 70 K kinetic measurements is much weaker at 30 K as the peak of the rotational state distribution shifts downward, so the $^rR_1(2.5)$ line near 7060 $cm^{-1}$ used for the 30 K measurements. At this frequency, the stability of the timing feedback and the resulting larger timing jitter of the ringdown events reduced the fraction of events within the 3.2-4.2 ms time window to about 40%. For this reason, the signal $I(t)$ in red is an average of about 400 events, while the background ringdown is still an average of about 15000 ringdown events.

Finally, we note that one can solve Eq 10 to give a closed form expression for $n(t)$ without presuming any functional form:

$$n(t) = \frac{-1}{c\sigma}\frac{L}{L_A}\frac{d}{dt}\ln[Ratio(t)]. \quad (15)$$

To reduce the measured ringdown data to a concentration profile in this way suffers from the noise-amplifying numerical differentiation of data which itself is derived from an increasingly noisy ratio of similarly decaying signals. We concur with the suggestion of Brown et al.[9] that using a parameterized fit to the ringdown ratio is a more stable approach when the functional form of $n(t)$ can be kinetically justified. The detailed treatment of the present data is discussed more fully in section 4.1 below.

### *3.4 CN(v=1) kinetics with added $O_2$*

We have measured the kinetics of formation and loss of rotationally thermalized CN(v=1) as a function of added $O_2$ in 70 K and 30 K flows using the methods described above. Figure 8 shows the background normalized ringdown ratios for a sequence of added $O_2$ in the two flows. At 70 K in figure 8(a), one sees the ringdown ratio to have a short period of negative curvature immediately after the time of laser photolysis at 23 μs, followed quickly by an extended region of declining positive curvature. This is the pattern of ringdown ratios characteristic of rising and falling CN concentrations, where the rate of decay increases at higher $O_2$ concentrations. Figure 8(c) illustrates the rise and fall kinetic curves, optimized to reproduce the corresponding ringdown ratios shown in figure 8(a). At 30 K in figure 8(b), the duration of the initial downward curvature is substantially enhanced, which corresponds to an extended period of growth in the thermalized CN(v=1) absorption prior to decay. The corresponding rise and fall curves fit to these ringdown ratios are illustrated in figure 8(d). The fall rates, when plotted against the $O_2$ density in Fig 10a and 10b,

give slopes with the dimensions of bimolecular rate coefficients as given in Table 2. The $O_2$ dependent rise rates are plotted in Figure 11a and 11b and are discussed along with the amplitudes in section 4.1 in the context of relaxation and reaction.

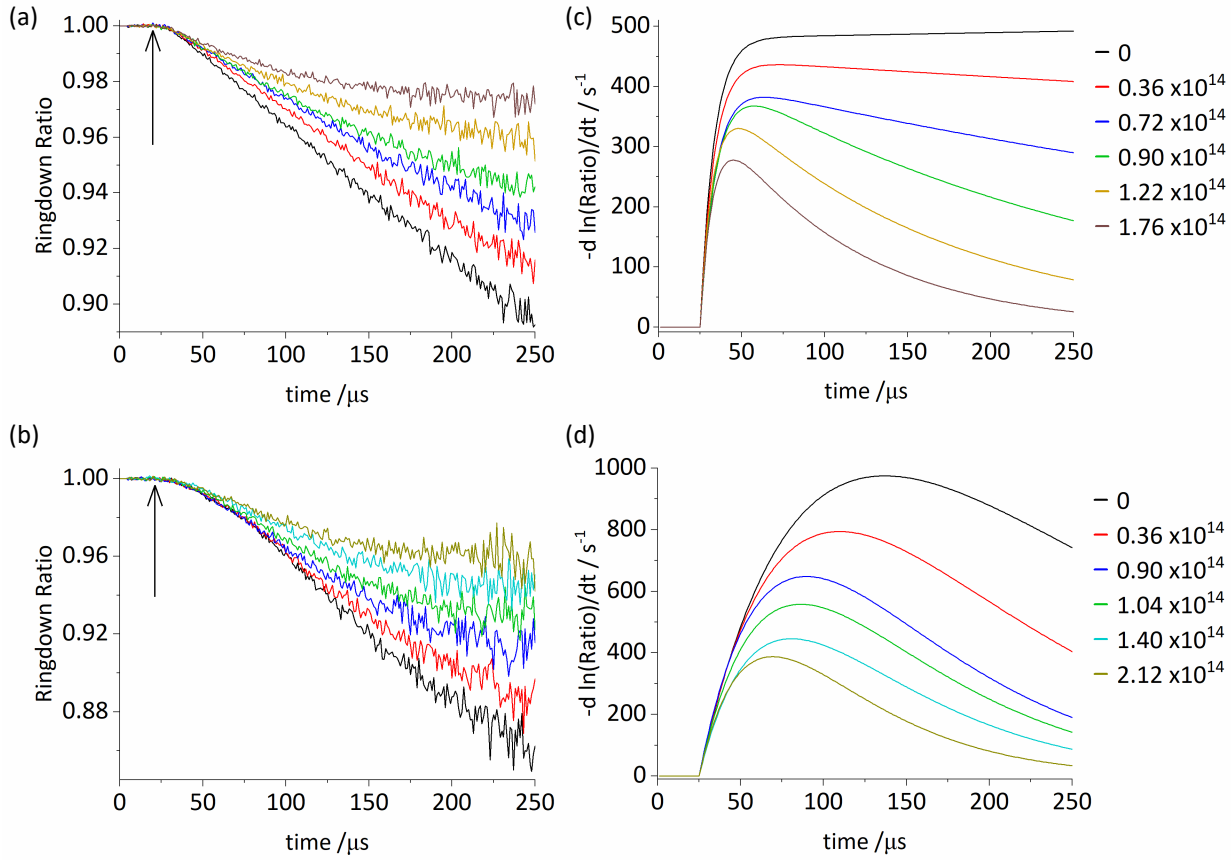


*Figure 8. Background normalized ringdown ratio for CN(v=1) with varying densities of $O_2$ at 70 K (a) and 30 K (b). Time dependent CN kinetics obtained from the three-parameter fit to the respective ringdown ratio in the 70 K (c) and 30 K (d) flow.*

### *3.5 CN(v=1) kinetics with added NO*

Analogous measurements were made with NO as the metered co-reactant instead of $O_2$ using the same two Laval nozzles. Figure 9 (a) and (b) shows the background normalized ringdown ratios as a function of added NO at 70 K and 30 K and figure 9 (c) and (d) shows the corresponding concentration profiles derived from fits to the ringdown ratios.

As with added $O_2$, the decay rates are found to vary linearly with the density of the co-reactant. Figures 10c and d show the effect of added NO on the fall rates extracted from the fits at the two temperatures. Figures 11c and d show the corresponding rise rates.

*Table 2. Summary of reaction flow conditions and apparent rate coefficients obtained for the removal of CN(v=1) by $O_2$ and NO. 30 K rate coefficients should be considered lower bounds (see text).*

| M | T / K | Gas | Flow density / $10^{16}$ molecule $cm^{-3}$ | [M] / $10^{14}$ molecule $cm^{-3}$ | No of measurements | $k$ / $10^{-11}$ $cm^3$ molecule$^{-1}$ $s^{-1}$ |
|---|---|---|---|---|---|---|
| $O_2$ | 71.3 ± 2.8 | $N_2$ | 5.5 | 0.44-5.12 | 8 | 2.49 ± 0.08 |
| | 30.6 ± 1.2 | Ne | 4.5 | 0.36-2.12 | 9 | 6.41 ± 0.23 |
| NO | 71.3 ± 2.8 | $N_2$ | 5.5 | 0.22-2.37 | 12 | 10.49 ± 1.05 |
| | 30.6 ± 1.2 | Ne | 4.5 | 0.27-1.71 | 7 | 15.73 ± 0.55 |

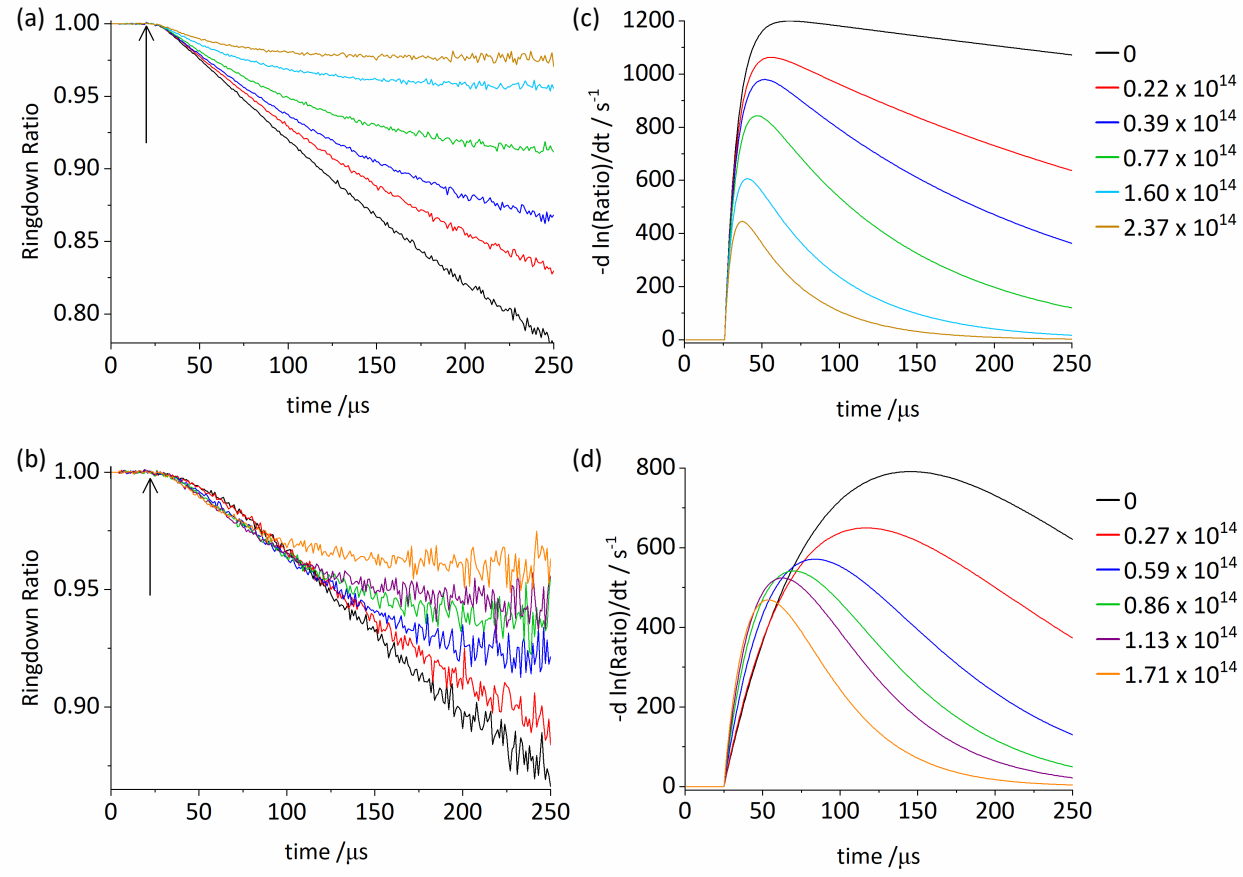


*Figure 9. Background normalized ringdown ratio for CN(v=1) with varying densities of NO at 70 K (a) and 30 K (b). Time dependent CN kinetics obtained from the three-parameter fit to the respective ringdown ratio in the 70 K (c) and 30 K (d) flow.*

The trends in the rise rates and the amplitudes reveal some interesting differences both with temperature and between NO and $O_2$ that will be discussed in section 4.1 in the context of thermalization. The apparent bimolecular rate coefficients derived from the slopes of $k_{fall}$ vs. the co-reactant density in figure 10 (a)-(d) are summarized along with the measurement conditions in Table 2.

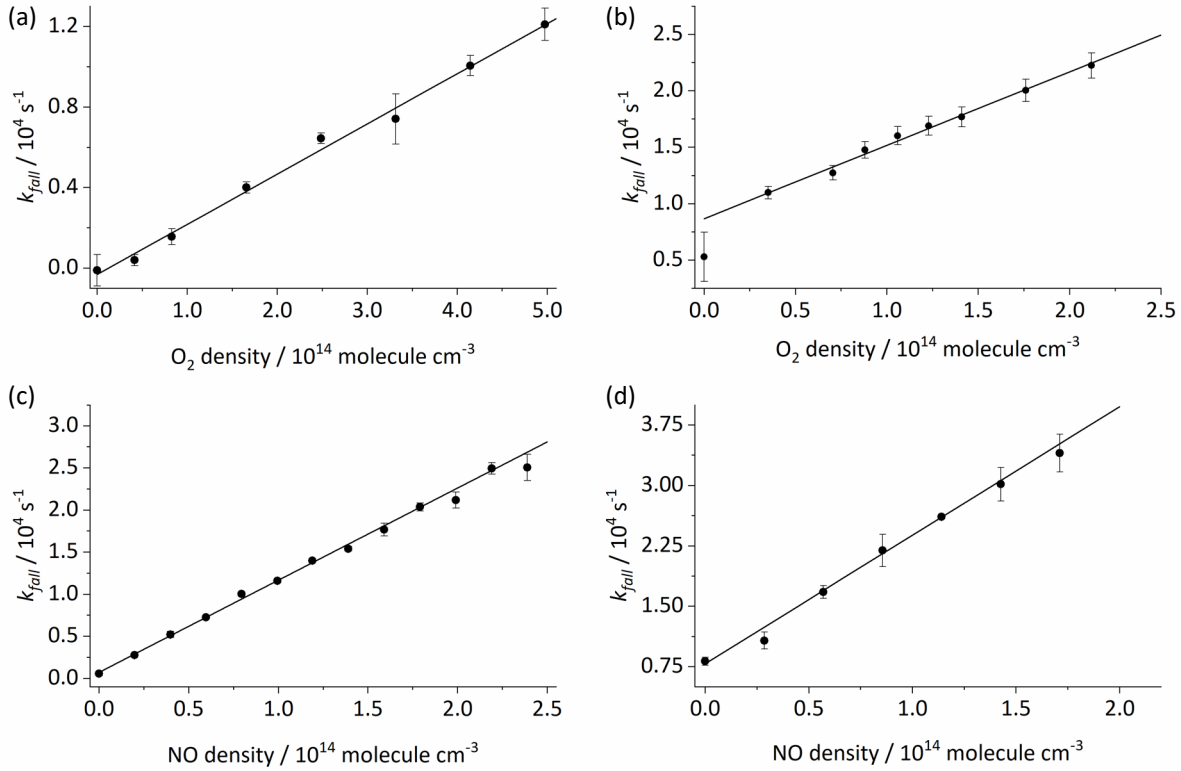


*Figure 10. Pseudo first order rate($k_{fall}$) coefficient for varying concentrations of $O_2$ in 70 K (a) and 30 K (b) flow and for varying concentrations of NO in 70 K (c) and 30 K (d) flow.*

We note that in the absence of co-reactant, the optimized difference-of-exponential functional form for the time-dependent thermalized CN (v=1) population is not flexible enough to fit the ringdown ratios accurately. The best-fit rate parameters in the absence of $O_2$ or NO are nonetheless included in figures 10 and 11 but given no weight in the slopes evaluated with the rest of the data, which is generally well-represented by the chosen functional form for the rise and fall.

## 4 Discussion

### *4.1 Delayed thermalization in CN (v=1)*

The use of 248 nm photodissociation of BrCN as a source of CN (v=1) for thermal kinetic studies requires that attention be paid to the relative timescales of formation, thermalization, and removal[45, 49-50, 55]. Even in collisional environments where rotational relaxation could normally be assured, a residual reservoir of

metastable highly excited rotational states can persist and affect the slower kinetics of vibrational relaxation or chemical reaction. Hay et al.[47] characterized the evolving bimodal rotational distributions of CN(v=0) following 193 nm dissociation of BrCN in several inert and reactive collisional environments at room temperature. Wright and Dagdigian[55] used BrCN photolysis in the presence of $O_2$ to investigate the rotational state dependence of reaction and rotational thermalization in CN(v=0) + $O_2$ collisions. Their observations provide a more global picture in v=0 of what we observe for v=1, since our spectral coverage is limited to a few low-J states of CN (v=1). As shown in Figure 5, in the absence of co-reactant, the initial population in these states is small and the relative populations among these levels correspond closely to the temperature of the gas flow as soon as the populations begin to grow. We at first anticipated that addition of small amounts of $O_2$ or NO would simply accelerate the removal of thermalized CN, which is what we observe in the 70 K measurements. At the lower temperature used here, the growth rates are slower and become more similar to the removal rates, calling for a more explicit treatment of the thermalization kinetics.

To represent the delayed thermalization of metastable high rotational states of CN (v=1) we consider a simplified kinetic model, analogous to the approach used by Wright & Dagdigian to investigate the rotational dependence of the reaction of CN(v=0) with $O_2$[55]. The evolving bimodal rotational distribution of CN rotational states following photolysis of BrCN is approximated as a two-component mixture of a thermalized fraction and a hot reservoir, with each component subject to effective rates of relaxation and reaction. Depicting the rotationally hot, metastable component of CN(v=1) as CN*, the thermalized component of CN(v=1) as CN, and the nonreactive carrier gas as M, the kinetic model has these steps:

CN* + M → CN + M  rotational thermalization by M; $k^*_{rot,M}$

CN* + $O_2$ → CN + $O_2$  rotational thermalization by $O_2$; $k^*_{rot,O_2}$

CN* + $O_2$→ removal by reaction or vibrational relaxation; $k^*_{O_2}$

CN + $O_2$ → removal by reaction or vibrational relaxation; $k_{O_2}$

CN → removal by background processes; $k^0_{fall}$

The photodissociation of BrCN produces no significant initial population of thermalized CN(v=1), which is formed exclusively by rotational thermalization of an initial concentration $n_0$ of hot CN*(v=1). Integrating the appropriate rate equations gives these time-dependent concentrations in the two-component model:

$$[CN^*] = n^0 \exp(-k_{rise}t)$$

$$[CN] = n^0 \frac{k^*_{rot,M}[M] + k^*_{rot,O_2}[O_2]}{k_{fall} - k_{rise}} \left[\exp(-k_{fall}t) - \exp(-k_{rise}t)\right]$$

where $$k_{rise} = k^*_{rot,M}[M] + \left(k^*_{rot,O_2} + k^*_{O_2}\right)[O_2]$$

and $$k_{fall} = k^0_{fall} + k_{O_2}[O_2].$$

Within this simplified kinetic model, $k_{rise}$ and $k_{fall}$ are two of the three parameters extracted from the SKaR analysis of the ringdown measurements and the gradients of these rates with respect to the added $O_2$ (or NO) concentrations give the bimolecular rate coefficients for total deactivation of the metastable CN* and the total removal rate constant for the thermalized CN (v=1) by $O_2$. Any contributions from population initially produced in higher or lower vibrational levels $v \neq 1$ are ignored, and the more complex, multi-exponential kinetics of a master equation to describe the rotational thermalization[56] is replaced with a single empirical rate process as a first approximation. The slow removal of CN in the absence of $O_2$ (or NO) due to diffusion, vibrational relaxation, or background reactions is represented by a slow exponential loss with the rate $k^0_{fall}$. An identical model is used for NO as a collision partner.

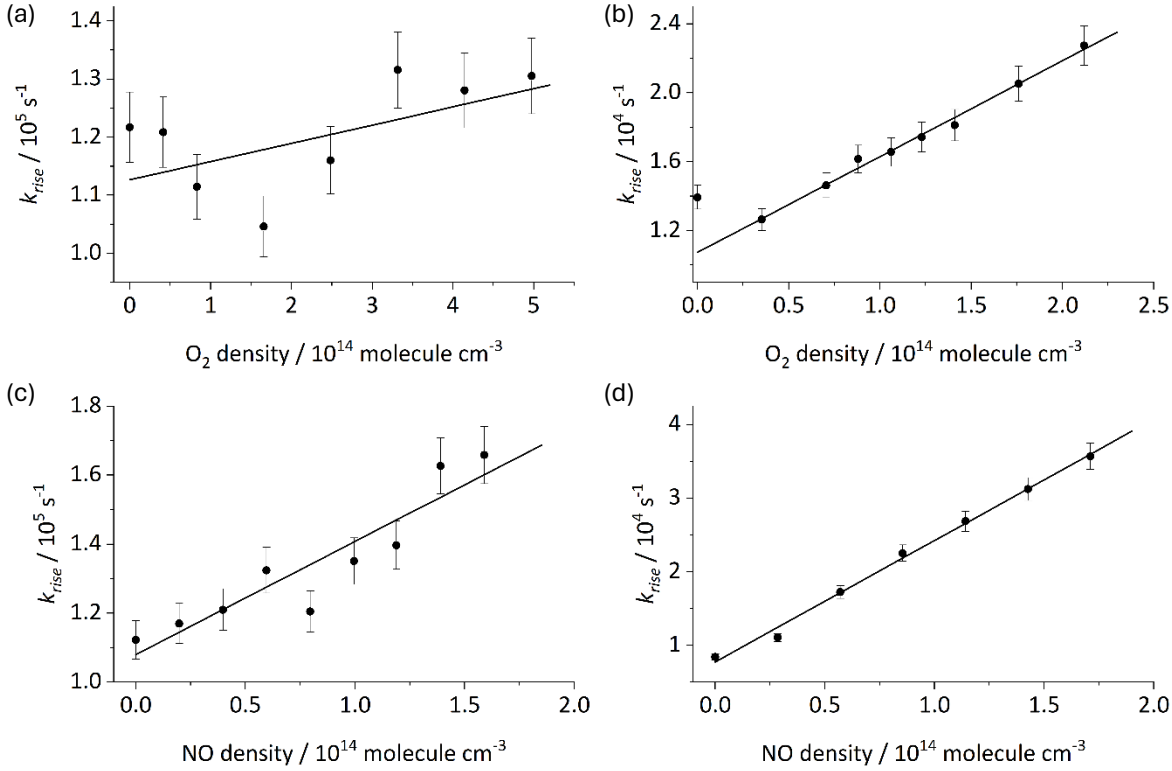


*Figure 11. CN(v=1) growth rate ($k_{rise}$) coefficient for varying concentrations of $O_2$ in 70 K (a) and 30 K (b) flow and for varying concentrations of NO in 70 K (c) and 30 K (d) flow.*

The amplitude of the [CN] rise and fall in this model depends on the added reagent $O_2$ (or NO) not only through the rise and fall rates, but also on the fraction $\phi$ of the total removal of CN* by $O_2$ that leads to the detected, thermalized CN(v=1): $\phi = \frac{k^*_{rot,O_2}}{k^*_{rot,O_2}+k^*_{O_2}}$

### *4.1.1 CN(v=1) + $O_2$ and NO at 70 K*

The growth rates extracted from the SKaR analysis of the kinetics of CN (v=1, J=5.5) in the 70 K $N_2$ flow at a density of 5.5 x $10^{16}$ $cm^{-3}$ are already close to our fastest resolvable growth rates and show only a poorly determined dependence on the added $O_2$. At the lowest $O_2$ densities, the decay is slow, and the growth is not well represented by a single exponential, as may be expected in the multi-exponential relaxation from a more detailed master equation description of the evolving state distribution[56]. When restricted to the three-parameter form of Eq 14, a best-fit rise rate is thus subject to relatively large errors, as seen from the scatter in Fig. 11a. The pattern of decreasing peak amplitudes as a function of added $O_2$ can be simulated to

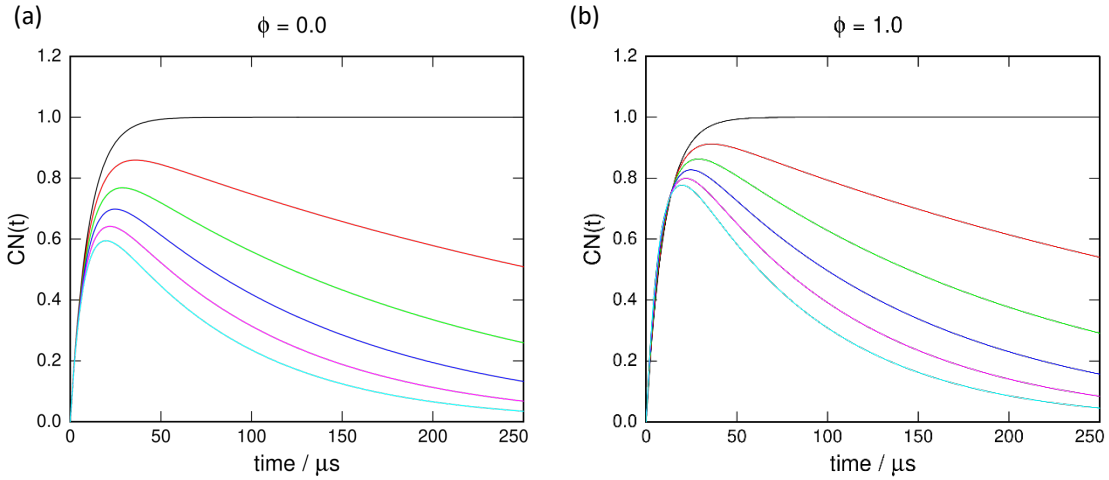


*Figure 12. The influence of the branching fraction φ on the simulated thermalization and removal of CN(v=1) by $O_2$ at 70 K for increasing $O_2$ number density. Rise and fall rates follow the experimental values, and the simulated kinetics are computed at six uniformly spaced $O_2$ density values from 0 to 5.12 x $10^{14}$ $cm^{-3}$, the maximum used in the measurements illustrated in figure 8a and 8c.*

assess the fate of the highly excited CN(v=1) that is removed by $O_2$. Within the two-state model described in Section 4.1, the rise and fall rates are unaffected by the branching between rotational relaxation within v=1 and removal of the hot CN, but the peak intensity will decrease more rapidly as the branching fraction decreases. Figure 12 illustrates this progression of intensities for the family of kinetic traces following the

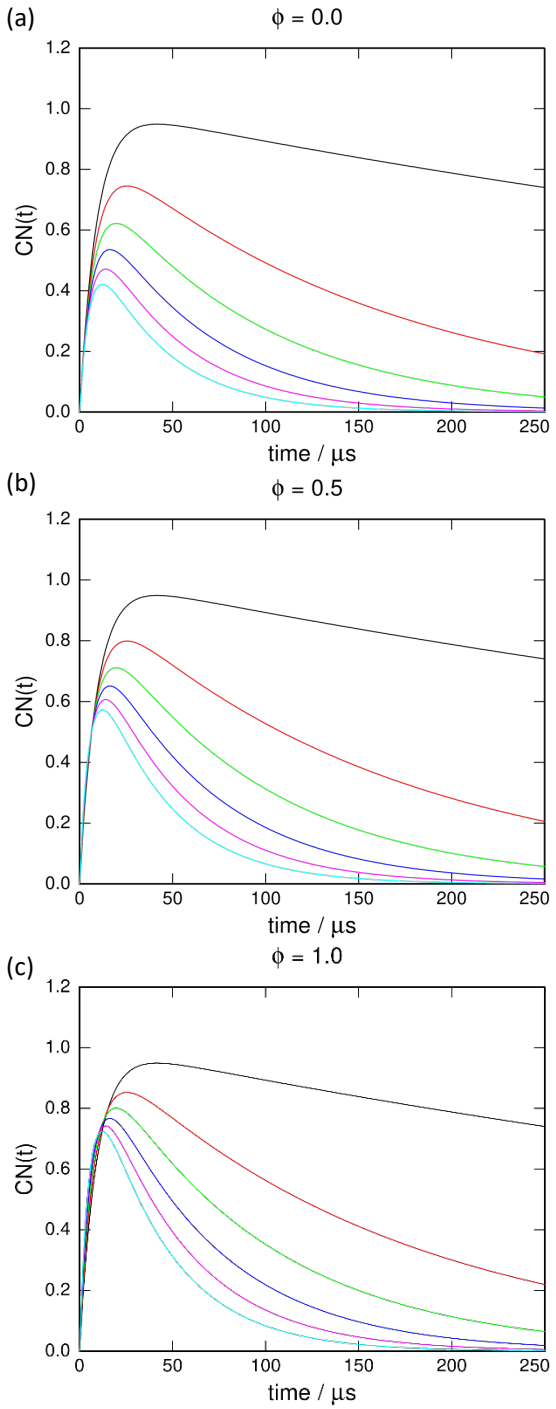


*Figure 13. The influence of the branching fraction φ on the simulated thermalization and removal of CN(v=1) by NO at 70 K for increasing NO number density. Rise and fall rates follow the experimental values, and the simulated kinetics are computed at six uniformly spaced NO density values from 0 to 2.5 x $10^{14}$ $cm^{-3}$, the maximum used in the measurements illustrated in figure 9a and 9c.*

$O_2$-dependent rise and fall rates determined from the rates shown in Figures 10a and 11a for the limiting cases of $\phi$ = 0 and 1. The observed rate of amplitude decrease is more consistent with $\phi$ = 0, where most of the removal of hot CN(v=1) by $O_2$ does not lead to thermalized CN(v=1).

As NO is added to the 70 K $N_2$ flow, the effective growth rates also increase systematically, as illustrated in Fig 11c. The gradient with respect to the NO concentration gives an effective bimolecular rate constant near 3 x $10^{-10}$ $cm^3$ $mol^{-1}$ $s^{-1}$, almost 200 times faster than the effective rotational thermalization rate by $N_2$ at this temperature. The two-state simulations using the observed rise and fall rates for NO are shown in figure 13 for $\phi$ = 0.0, 0.5, and 1.0. When $\phi$=1, all of the initial population initially in the rotationally hot CN(v=1) proceeds eventually through the thermalized CN(v=1) and the peak amplitude drops with increasing NO concentration only due to the increase in the removal rate. When $\phi$ <1, some of the rotationally hot CN(v=1) is diverted directly out of v=1 through vibrational relaxation by NO without ever contributing to the thermalized CN(v=1) signal, resulting in a more rapid decrease in the peak amplitude with [NO] as $\phi$ is decreased. An intermediate value of $\phi$ = 0.5 more closely resembles the measured attenuation of the intensities with added NO at 70K, as illustrated in figure 9c. The same qualitative mechanism of decreased amplitude would exist in a more realistic treatment of multi-state

thermalization. Despite the model simplifications, it seems likely that although $O_2$ is at least as efficient as NO at removing the (unseen) highly excited states of CN(v=1), $O_2$ is less effective at inducing pure rotational relaxation within v=1 than is NO, based on the more rapid reduction in amplitudes with added $O_2$ than with NO. This is consistent with Smith's arguments discussed in Section 4.2 that the absence of a pressure dependence for the reaction suggests that the primary fate of the NCOO complexes is reaction.

For both sets of measurements at 70 K, the rise and fall rates are well separated at all co-reactant concentrations, and although the growth kinetics have been oversimplified in the modelling, it seems unlikely that significant continuing relaxation from a persistent hot reservoir can be causing the observed fall rate to be slower than the true removal rate for thermalized CN(v=1).

### *4.1.2 CN(v=1) + $O_2$ and NO at 30 K*

The growth of rotationally thermalized CN(v=1) is at least 5 times slower in the colder flow, consisting of Ne at 4.5 x $10^{16}$ $cm^{-3}$ at 30K, compared to the $N_2$ flow at 70K and similar density. Within the observable time window of about 250 μs for uniform flow kinetics, the thermalized reactions of primary interest cannot be observed in temporal isolation from a nearly completed thermalization step using BrCN as a photolytic precursor, a limitation that has led us to the model of competing relaxation and reaction developed above. Other researchers have used different CN precursors such as NCNO[17, 20, 25, 57], NCCN[30, 58-60], or $CH_3COCN$[53, 61], for which the nascent CN state distribution lacks the extremely high rotational states and is more readily thermalized, minimizing this interference. The translational relaxation of fast CN photofragments proceeds faster than the rotational thermalization and has been explored in detail by Alagappan, et al. using ICN photolysis and a variety of collision partners[62]. We found the trends in thermalization at low temperatures with BrCN interesting and worth exploring in their own right, while still providing data relevant to the low temperature thermal rates for the vibrationally excited CN radicals.

The SKaR analysis of the CN (v=1, N=2, J=2.5) kinetics with added $O_2$ in the 30 K Ne flow leads to similar values of $k_{rise}$ and $k_{fall}$, both increasing linearly with [$O_2$]. Figure 11b shows the variation of $k_{rise}$ with [$O_2$] for this set of measurements. The gradient gives an effective removal rate constant for CN*(v=1) by $O_2$ of 5.5x$10^{-11}$ $cm^3$ $mol^{-1}$ $s^{-1}$, fast enough to double the rise rate with the addition of 0.5% $O_2$ to the Ne flow.

Simulations to assess the fate of the CN*(v=1) following removal by $O_2$ at 30K are shown in figure 14, using the concentration-dependent rates derived from the experiment. In this case, the $\phi = 0$ limit is a good

description of the observed pattern of amplitudes, suggesting that the enhanced removal of CN*(v=1) by $O_2$ is primarily reactive or vibrationally inelastic. If rotational relaxation within CN(v=1) were the dominant pathway for the CN*(v=1) removal by $O_2$, the amplitudes would decrease much more slowly, as depicted in the $\phi = 1$ case. It is interesting to contrast this behavior with that found in the room temperature measurements of Wright and Dagdigian, who followed the rotational distribution of CN(v=0) by LIF as a function of time following 193 nm photodissociation of BrCN in a pure $O_2$ environment. They found a persistence of total (rotationally summed) CN(v=0) during the time when the bimodal rotational distribution of CN(v=0) was being relaxed that indicated that the reactive loss of CN*(v=0) through collisions with $O_2$ was significantly slower than both the rotational relaxation and the reaction of thermalized CN(v=0). From a two-state model similar to the one we use, they found an effective rotational relaxation rate constant of $1.8 \times 10^{-11}$ $cm^3$ $molecule^{-1}$ $s^{-1}$, about 70% as fast as the thermal rate of reaction with $O_2$ and about 18 times faster than the apparent rate of reaction with the rotationally hot CN(v=0). At the reduced temperature of our measurements, we find little evidence for efficient pure rotational relaxation by of rotationally hot CN(v=1) by $O_2$, unlike in CN(v=0) at room temperature. In addition, the acceleration of the thermal CN(v=1) growth rate with added $O_2$ suggests that the deactivation of the rotationally hot CN(v=1) by $O_2$ by reactive or vibrational relaxation pathways occurs with a rate constant comparable to that of the removal of thermalized CN(v=1) by $O_2$ at 70K.

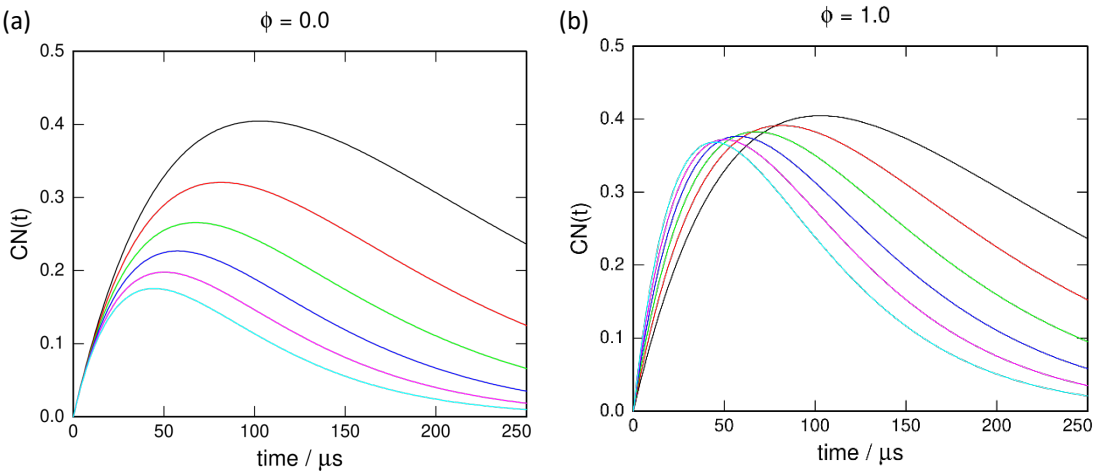


*Figure 14. The influence of the branching fraction φ on the simulated thermalization and removal of CN(v=1) by $O_2$ at 30 K for increasing $O_2$ number density. Rise and fall rates follow the experimental values, and the simulated kinetics are computed at six uniformly spaced $O_2$ density values from 0 to $2.12 \times 10^{14}$ $cm^{-3}$, the maximum used in the measurements illustrated in figure 8b and 8d.*

The addition of NO to the 30 K Ne flow accelerates both $k_{rise}$ and $k_{fall}$ in a way that is qualitatively similar to $O_2$, but the pattern of amplitudes is different. Figure 11d shows the gradient of $k_{rise}$ with respect to [NO] to be about three times larger than the effective removal rate of CN*(v=1) by $O_2$ in the same 30 K flow. The

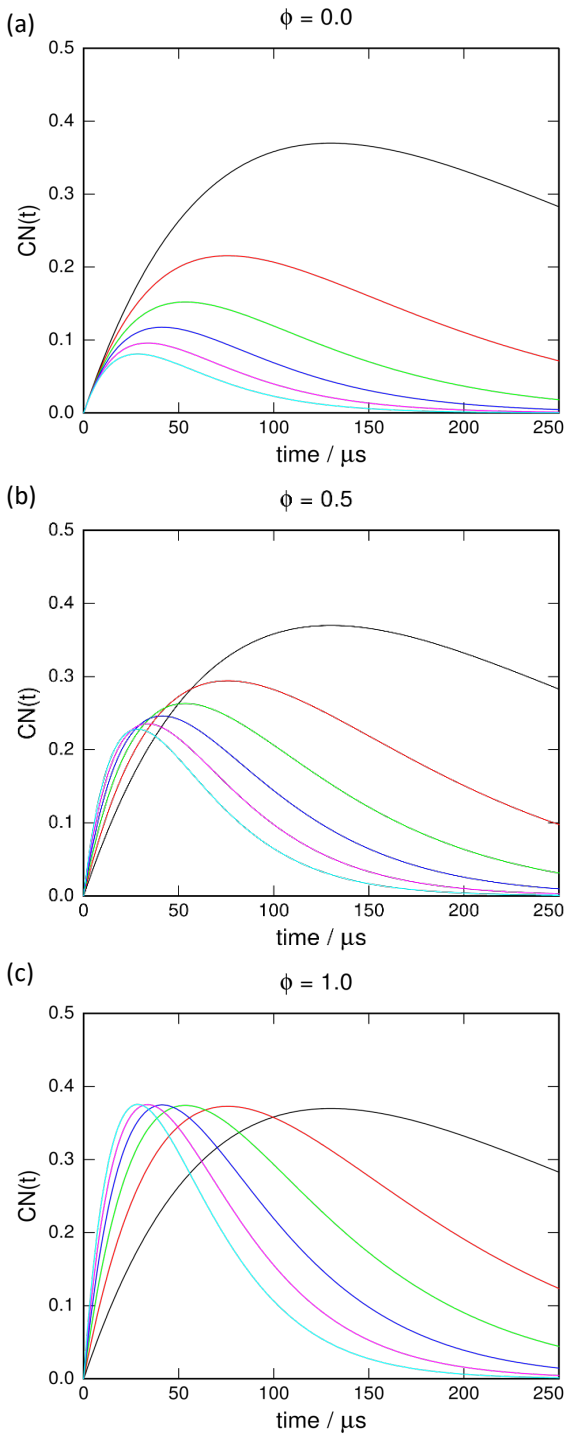


*Figure 15. The influence of the branching fraction φ on the simulated thermalization and removal of CN(v=1) by NO at 30 K for increasing NO number density. Rise and fall rates follow the experimental values, and the simulated kinetics are computed at six uniformly spaced NO density values from 0 to 1.71 x $10^{14}$ $cm^{-3}$, the maximum used in the measurements illustrated in figure 9b and 9d. The observed pattern of amplitudes most closely resembles the simulation with φ=0.5.*

increase in the absolute amplitudes of the time-dependent CN(v=1) signals with increasing [NO] prior to the time of maximum signal seen in figure 9d is consistent with a significant fraction of the loss of CN*(v=1) leading to rotational thermalization in CN(v=1). Figure 15 shows the corresponding simulations for [NO]-dependent [CN(v=1)] kinetics for $\phi = 0$, 0.5 and 1.0, using the experimentally determined $k_{rise}$ and $k_{fall}$ for the 30 K measurements with NO. As for the 70 K measurements with NO, the intermediate value of $\phi$ more closely resembles the measurements, unlike with $O_2$, where rotational thermalization seems not to contribute significantly to the total removal rate of CN*(v=1) by $O_2$.

Even though the second order plots of $k_{fall}$ vs the added co-reactant $O_2$ or NO produce apparently compelling straight-line fits, the confounding effect of slow thermalization makes the identification of the slopes with the desired removal rate for thermalized CN(v=1) suspect. We have explored a somewhat more realistic model of rotational relaxation including an intermediate group of rotational levels in addition to the thermal and metastable group, in an attempt to estimate the range of observable kinetic consequences. General solutions for the growth and decay of the rotationally thermalized population in this three-state model do not typically give single exponential rise and fall kinetics for arbitrarily chosen relaxation and reaction rate coefficients. It is, however, possible to choose a constrained set of rate

constants and initial populations in the CN levels that continues to feed population from the metastable reservoir into the thermalized CN during its decay that can mimic a two-state model with comparable rise and fall rates that also scale linearly with reactant density. Identifying the slope of the empirical decay rate vs reactant density with the thermal removal rate constant would underestimate the true thermal rate constant by as much as a factor of 2 by oversimplifying the slow relaxation kinetics and failing to recognize a persistent source term. The details of such a model are underdetermined by our measurements but suggest to us that the apparent bimolecular rate coefficients derived from the 30 K measurements are a lower bound to the true thermal removal rates and could be as much as a factor of 2 slower than the true value. Thus, although we report the values for the 30 K rate coefficients from the two-component analysis, we note these should be viewed as lower bounds. In retrospect, a different CN(v=1) photolytic precursor might have produced more easily interpreted results at very low temperature.

### *4.2 Implications of the bimolecular rates*

The reaction of CN with $O_2$ is perhaps the best-studied "radical-radical" reaction while reaction with NO offers an interesting contrast in that there is no reactive pathway open, and the NCNO adduct plays a key role. Reaction involving CN(v=1) has also been examined to a more limited extent with these target reactants, and the results further highlight the marked differences in their behavior. The reaction dynamics and kinetics of CN with $O_2$ have been summarized in a comprehensive review by Ian Smith[63]. Kinetics have been measured over a wide range of temperatures, and the reaction has also intrigued theorists as a prototype barrierless recombination reaction for which abundant experimental data is available. Early theory only considered the long-range potential, either as dipole-quadrupole electrostatics[64] or including dispersion interactions[26-27]. These gave mildly positive temperature dependent rates that were considerably above the measurements, coming close to agreement at the lowest measured temperature. The disagreement with the measured rates then motivated Kim and Klippenstein[29] to include a treatment of the region of incipient chemical interaction from 1.7 to 3 Å and apply variational statistical calculations for the entrance channel to the NCOO adduct. The calculated rates then showed the correct form of the temperature dependence, increasing rapidly as temperature decreased down to 50 K, the lowest they felt suitable for treatment with their methods. Quantitative agreement with the low temperature experimental measurements was not achieved nor expected given the approximate nature of their potential. A related treatment was reported by Vallance and coworkers[34] who used G2-level theory to characterize aspects of the potential surface along with classical trajectories for the entrance channel, and variational RRKM theory

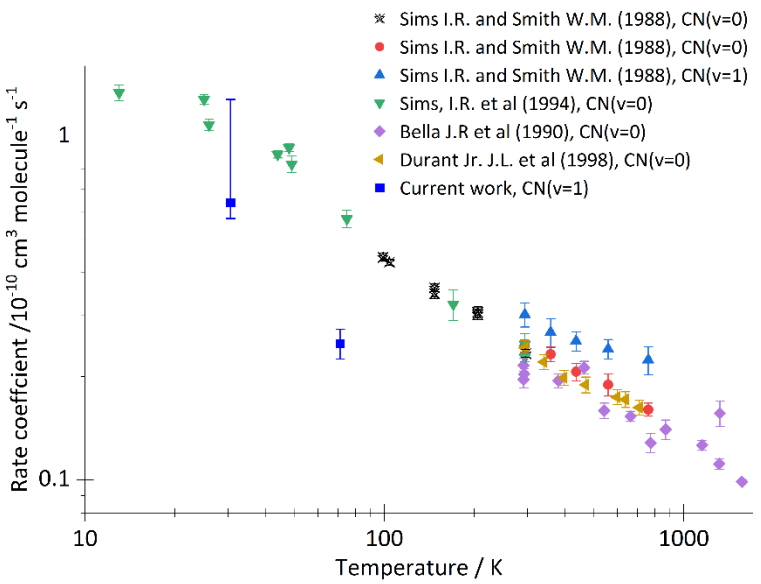


*Figure 16. Log –log plot of temperature vs bimolecular rate for the reaction of CN + $O_2$ in comparison with data presented in the literature and the rate measure using the UFCRDS method. Adapted from ref 36.*

to assess the branching between reaction and decay back to reactants. They noted the challenge of matching the experimental rates at low temperature and suggest, following Kim and Klippenstein, that the electronic degeneracy factor of 1/3 may be increased if intersystem crossing plays a role at long range, becoming important at low temperature.

This is all prologue to the discussion of the thorny problem of the low temperature rate for CN(v=1) + $O_2$. For this reaction we measured the rate coefficient at 70 K to be $2.49 \pm 0.08 \times 10^{-11}$ cm$^3$ molecule$^{-1}$ s$^{-1}$. This is the first such measurement below room temperature, and it is on the order of half the rate reported by Sims and Smith for CN (v=0) at these temperatures, a large and surprising discrepancy. Relative rates for CN(v=1)/CN(v=0) reaction with $O_2$ have been measured at a range of temperatures by four groups with conflicting results. The most comprehensive measurements are from Atakan et al. and Sims and Smith. Atakan et al. measured these rates from 300 to 1000 K and found CN(v=1) to be consistently 30% slower than v=0. Sims and Smith, on the other hand, measured the ratio in a similar temperature range and found the (v=1) rates to be 25% higher. It has been suggested that the (v=1) rates could be faster if the vibrational excitation promotes dissociation of the NCOO adduct back to reactants with concomitant vibrational relaxation. Smith has argued, however, that the lack of pressure dependence to this reaction suggests that the dissociation to NCO + O must be too fast for this to play a role. Instead, he proposes that the increased rate they observe for v=1 results from the impact of C-O bond formation on the frequency of the CN vibration and the difference in slope, and the associated variational transition state, of these adiabatic curves. One prediction of this view is that the enhanced rate for (v=1) would disappear at low temperature when the rate is entirely determined at long range. Our results are clearly inconsistent with this extrapolation of their results, although it must be said we have not measured the (v=0) rate so we have not determined this ratio directly. If we were to assume that the (v=1) and (v=0) rates should be equal at low temperature as suggested by Smith, then we find our measurements disagree by more than five times the mutual uncertainty. It is difficult to imagine systematic errors that

could account for this discrepancy, at least for our 70 K result. Sadly, although Smith had called for low temperature measurements of the $O_2$ (v=1) rates as important to illuminate this key open question for the CN + $O_2$ system, it seems full clarity is not yet achieved with the present measurement.

The bound NCNO system is much better characterized than NCOO: detailed photochemistry studies have been performed and all show formation of cold radical products near the threshold of dissociation[41]. It has a deeper well as shown in figure 1 and no competing reactive pathways. In contrast to the reaction with $O_2$, the loss of CN(v=1) in the presence of NO is much faster compared at the temperatures studied: at 70 K we find it to be (10.49 ± 1.05) × $10^{-11}$ $cm^3$ $molecule^{-1}$ $s^{-1}$. Previously reported rates generally show a negative temperature dependence. Sims et al. [17] studied the rate of reaction of CN(v=1) with NO for the temperature range of 296 to 761 K and found it followed the trend $k = 7.6 \times 10^{-11} (T/298)^{-0.30}$, where $k$ is the bimolecular rate and $T$ is the temperature. When this relationship is extended to lower temperatures, it holds for our measured rate at 70 within the limits of uncertainties (figure 17).

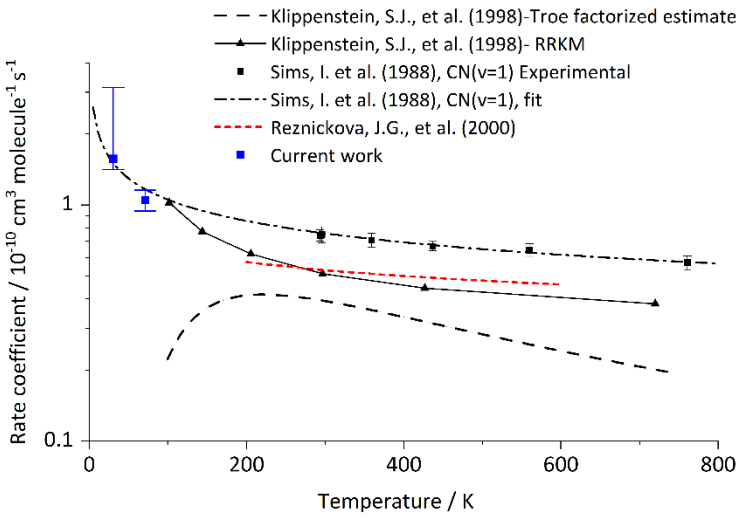


*Figure 17. Comparison of the bimolecular rate measured with UF-CRDS for the reaction of CN with NO vs literature. Adapted from ref 39 and 65.*

The close connection between the high-pressure limit for the CN + NO association rate coefficient and the quenching rate for CN(v=1) has been noted by Klippenstein et al. in a joint experimental/theoretical study of the pressure dependence of the reaction[39]. The theoretical treatment is complicated both by the possible reaction on the triplet surface and by the participation of the CNNO isomer of the complex which is readily accessible. They applied an RRKM treatment with a variational outer TS at 5-10 Å that includes an electronic degeneracy factor of 4 to 8 to account for the triplet surface contribution, and a conventional inner transition state with a degeneracy factor of unity. They examined the pressure dependence at a range of temperatures from 207 to 740 K and pressures up to 900 torr. Their results were consistent with the lower pressure measurements of Sims and Smith[17], and the theory matched experiment when strongly temperature-dependent values for $\Delta E$ down were employed. These pressures did not take them near the

high-pressure limit, however. Reznickova and coworkers subsequently extended the same manner of analysis and experiment up to 100 bar to map the fall-off curves to this limit[65]. Their analysis led to an expression for the high-pressure limit that was independent of temperature and is a factor of two lower than our value at 70 K. They also directly measured the CN(v=1) relaxation induced by collision with NO and found the rate agreed well with their high-pressure limit for the association reaction, although with a mild negative temperature dependence:

$$k = (5.3\pm1.3) \times 10^{-11}(T/300)^{-0.2\pm0.2}\ \text{cm}^3\ \text{s}^{-1}.$$

This is also plotted in Fig. 17 and is in agreement with our determination within their estimated uncertainty. Reznickova and coworkers compared the experimental measurements with two alternative model treatments and the VTST approach of Klippenstein. All agreed reasonably well in the high temperature regimes of the experiments. Reznickova suggested low temperature measurements could be important to distinguish between them as their simplified statistical adiabatic channel model (SACM) was almost independent of temperature, while the classical trajectory SACM model showed a mild positive temperature dependence. Both disagree with our 70 K measurement, but the latter more so. Remarkably, the VTST approach of Klippenstein using shows a low temperature trend consistent with our measurement, though they did not report an extrapolation to 70 K. This is also shown in Fig. 17.

## 5 Conclusions

In the present paper we report the rate coefficients for reaction of vibrationally excited CN(v=1) with $O_2$ and NO at 70 measured using UF-CRDS. The rates of these reactions, both of which are fast at low temperature, are comparable to the time interval at which a ringdown decays; thus, we were able to successfully implement the SKaR method to measure them. The measured rate coefficient for CN(v=1) with $O_2$ at 70 is $(2.49 \pm 0.08) \times 10^{-11}$ cm$^3$ molecule$^{-1}$ s$^{-1}$. However, this is much lower than that reported by Sims et al. for CN(v=0) in a similar temperature range where they are expected to be similar. The rate coefficient measured for the non-reactive relaxation with NO at 70 K is $(10.49 \pm 0.22) \times 10^{-11}$ cm$^3$ molecule$^{-1}$ s$^{-1}$. The latter is discussed in the context of high-pressure limit rates for the association reaction and vibrational relaxation measurements at higher temperature. These measurements are complicated by the formation of a metastable population of high-*J* CN formed in the photolysis of the precursor BrCN which is partially relaxed to the probed CN levels by the target coreactants. This interference becomes more problematic at low temperatures, especially for NO, and a simplified kinetic model is developed to examine these effects. We

have also detailed important changes made to the data acquisition in the instrument that have increased throughput and stability.

## 6 Acknowledgments

This material is based upon work supported by the NSF under award number CHE-2247776. The contributions of GEH, as a senior scientist emeritus at BNL, have not been directly supported by any specific BNL or DOE funded program.

## 7 References


1. Rowe, B.; Dupeyrat, G.; Marquette, J.; Gaucherel, P., Study of the Reactions N+ 2+ 2n2→ N+ 4+ N2 and O+ 2+ 2o2→ O+ 4+ O2 from 20 to 160 K by the Cresu Technique. *J. Chem. Phys.* **1984**, *80*, 4915-4921.

2. Atkinson, D. B.; Smith, M. A., Design and Characterization of Pulsed Uniform Supersonic Expansions for Chemical Applications. *Rev. Sci. Instrum.* **1995**, *66*, 4434-4446.

3. Rowe, B.; Marquette, J., Cresu Studies of Ion/Molecule Reactions. *Int. J. Mass Spectrom. Ion Processes* **1987**, *80*, 239-254.

4. Sims, I.; Queffelec, J. L.; Defrance, A.; Rebrion-Rowe, C.; Travers, D.; Bocherel, P.; Rowe, B.; Smith, I. W., Ultralow Temperature Kinetics of Neutral–Neutral Reactions. The Technique and Results for the Reactions Cn+ O2 Down to 13 K and Cn+ Nh3 Down to 25 K. *J. Chem. Phys.* **1994**, *100*, 4229-4241.

5. Atkinson, D. B.; Smith, M. A., Radical-Molecule Kinetics in Pulsed Uniform Supersonic Flows: Termolecular Association of Oh+ No between 90 and 220 K. *J. Phys. Chem.* **1994**, *98*, 5797-5800.

6. Lee, S.; Hoobler, R. J.; Leone, S. R., A Pulsed Laval Nozzle Apparatus with Laser Ionization Mass Spectroscopy for Direct Measurements of Rate Coefficients at Low Temperatures with Condensable Gases. *Rev. Sci. Instrum.* **2000**, *71*, 1816-1823.

7. Oldham, J. M.; Abeysekera, C.; Joalland, B.; Zack, L. N.; Prozument, K.; Sims, I. R.; Park, G. B.; Field, R. W.; Suits, A. G., A Chirped-Pulse Fourier-Transform Microwave/Pulsed Uniform Flow Spectrometer. I. The Low-Temperature Flow System. *J. Chem. Phys.* **2014**, *141*, 154202.

8. Suas-David, N.; Thawoos, S.; Suits, A. G., A Uniform Flow–Cavity Ring-Down Spectrometer (Uf-Crds): A New Setup for Spectroscopy and Kinetics at Low Temperature. *J. Chem. Phys.* **2019**, *151*, 244202.

9. Brown, S. S.; Ravishankara, A.; Stark, H., Simultaneous Kinetics and Ring-Down: Rate Coefficients from Single Cavity Loss Temporal Profiles. *J. Phys. Chem. A* **2000**, *104*, 7044-7052.

10. Thawoos, S.; Hall, G. E.; Cavallotti, C.; Suits, A. G., Kinetics of Cn (V= 1) Reactions with Butadiene Isomers at Low Temperature by Cw-Cavity Ring-Down in a Pulsed Laval Flow with Theoretical Modelling of Rates and Entrance Channel Branching. *Faraday Discuss.* **2023**.

11. Rowe, B.; Dupeyrat, G.; Marquette, J.; Smith, D.; Adams, N.; Ferguson, E., The Reaction O+ 2+ Ch4→ Ch3o+ 2+ H Studied from 20 to 560 K in a Supersonic Jet and in a Sift. *J. Chem. Phys.* **1984**, *80*, 241-245.

12. Sims, I.; Smith, I.; Clary, D.; Bocherel, P.; Rowe, B., Ultra-Low Temperature Kinetics of Neutral–Neutral Reactions: New Experimental and Theoretical Results for Oh+ Hbr between 295 and 23 K. *J. Chem. Phys.* **1994**, *101*, 1748-1751.

13. Sims, I. R.; Smith, I. W., Rate Constants for the Radical-Radical Reaction between Cn and O2 at Temperatures Down to 99 K. *Chem. Phys. Lett.* **1988**, *151*, 481-484.

14. De Juan, J.; Smith, I. W.; Veyret, B., Kinetics of Cn (V= 0) and Cn (V= 1) with H2 Hcl and Hbr. *Chem. Phys. Lett.* **1986**, *132*, 108-112.

15. Sims, I. R.; Queffelec, J.-L.; Travers, D.; Rowe, B. R.; Herbert, L. B.; Karthäuser, J.; Smith, I. W., Rate Constants for the Reactions of Cn with Hydrocarbons at Low and Ultra-Low Temperatures. *Chem. Phys. Lett.* **1993**, *211*, 461-468.

16. Saidani, G.; Kalugina, Y.; Gardez, A.; Biennier, L.; Georges, R.; Lique, F., High Temperature Reaction Kinetics of Cn (V= 0) with C2h4 and C2h6 and Vibrational Relaxation of Cn (V= 1) with Ar and He. *J. Chem. Phys.* **2013**, *138*, 124308.

17. Sims, I. R.; Smith, I. W., Pulsed Laser Photolysis–Laser-Induced Fluorescence Measurements on the Kinetics of Cn (V= 0) and Cn (V= 1) with O 2, Nh 3 and No between 294 and 761 K. *J. Chem. Soc., Faraday Trans. 2* **1988**, *84*, 527-539.

18. Sims, I. R.; Smith, I. W. M., Pressure and Temperature Dependence of the Rate of Reaction between Cn Radicals and No over the Range 99⩽ T/K⩽ 450. *J. Chem. Soc., Faraday Trans.* **1993**, *89*, 1-5.

19. Sleiman, C.; El Dib, G.; Talbi, D.; Canosa, A., Gas Phase Reactivity of the Cn Radical with Methyl Amines at Very Low Temperatures (23–297 K): A Combined Experimental and Theoretical Investigation. *ACS Earth Space Chem.* **2018**.

20. Carty, D.; Le Page, V.; Sims, I. R.; Smith, I. W., Low Temperature Rate Coefficients for the Reactions of Cn and C2h Radicals with Allene (Ch2□ C□ Ch2) and Methyl Acetylene (Ch3c□ Ch). *Chem. Phys. Lett.* **2001**, *344*, 310-316.

21. Gupta, D.; Cheikh Sid Ely, S.; Cooke, I. R.; Guillaume, T.; Abdelkader Khedaoui, O.; Hearne, T. S.; Hays, B. M.; Sims, I. R., Low Temperature Kinetics of the Reaction between Methanol and the Cn Radical. *J. Phys. Chem. A* **2019**, *123*, 9995-10003.

22. Gardez, A.; Saidani, G.; Biennier, L.; Georges, R.; Hugo, E.; Chandrasekaran, V.; Roussel, V.; Rowe, B.; Reddy, K.; Arunan, E., High-Temperature Kinetics of the Reaction between Cn and Hydrocarbons Using a Novel High-Enthalpy Flow Tube. *Int. J. Chem. Kinet.* **2012**, *44*, 753-766.

23. Berteloite, C.; Lara, M.; Bergeat, A.; Le Picard, S. D.; Dayou, F.; Hickson, K. M.; Canosa, A.; Naulin, C.; Launay, J.-M.; Sims, I. R., Kinetics and Dynamics of the S (D 2 1)+ H 2→ Sh+ H Reaction at Very Low Temperatures and Collision Energies. *Phys. Rev. Lett.* **2010**, *105*, 203201.

24. Potapov, A.; Canosa, A.; Jiménez, E.; Rowe, B., Uniform Supersonic Chemical Reactors: 30 Years of Astrochemical History and Future Challenges. *Angew. Chem. Int. Ed.* **2017**, *56*, 8618-8640.

25. Sims, I.; Queffelec, J.; Defrance, A.; Rebrion-Rowe, C.; Travers, D.; Rowe, B.; Smith, I., Ultra-Low Temperature Kinetics of Neutral–Neutral Reactions: The Reaction Cn+ O2 Down to 26 K. *J. Chem. Phys.* **1992**, *97*, 8798-8800.

26. Clary, D. C.; Stoecklin, T. S.; Wickham, A. G., Rate Constants for Chemical Reactions of Radicals at Low Temperatures. *J. Chem. Soc., Faraday Trans.* **1993**, *89*, 2185-2191.

27. Stoecklin, T.; Dateo, C.; Clary, D., Rate Constant Calculations on Fast Diatom–Diatom Reactions. *J. Chem. Soc., Faraday Trans.* **1991**, *87*, 1667-1679.

28. Durant Jr, J.; Tully, F. P., Kinetic Study of the Reaction between Cn and O2 from 295 to 710 K. *Chem. Phys. Lett.* **1989**, *154*, 568-572.

29. Klippenstein, S. J.; Kim, Y. W., Variational Statistical Study of the Cn+ O2 Reaction Employing Ab Initio Determined Properties for the Transition State. *J. Chem. Phys.* **1993**, *99*, 5790-5799.

30. Balla, R. J.; Casleton, K. H., Kinetic Study of the Reactions of Cyanyl Radical with Oxygen and Carbon Dioxide from 292 to 1500 K Using High-Temperature Photochemistry. *J. Phys. Chem.* **1991**, *95*, 2344-2351.

31. Macdonald, R. G.; Argonne, K. L.; Sonnenfroh, D. M.; Liu, D.-J., Crossed-Beam Studies of Radical Reaction Dynamics. *Can. J. Chem.* **1994**, *72*, 660-672.

32. Mohammad, F.; Morris, V. R.; Fink, W. H.; Jackson, W. M., On the Mechanism and Branching Ratio of the Cn+ O2→ Co+ No Reaction Channel Using Transient Ir Emission Spectroscopy. *J. Phys. Chem.* **1993**, *97*, 11590-11598.

33. Qu, Z.-w.; Zhu, H.; Li, Z.-s.; Zhang, X.-k.; Zhang, Q.-y., Theoretical Study on the Mechanism of the Reaction between Cn and O2. *Chem. Phys. Lett.* **2002**, *353*, 304-309.

34. Vallance, C.; Maclagan, R. G.; Phillips, L. F., Numerical Study of the Reaction of Cn with O2. *Chem. Phys. Lett.* **1996**, *250*, 59-65.

35. Townsend, D.; Lahankar, S. A.; Lee, S. K.; Chambreau, S. D.; Suits, A. G.; Zhang, X.; Rheinecker, J.; Harding, L.; Bowman, J. M., The Roaming Atom: Straying from the Reaction Path in Formaldehyde Decomposition. *Science* **2004**, *306*, 1158-1161.

36. Smith, I. W., The Temperature-Dependence of Elementary Reaction Rates: Beyond Arrhenius. *Chem. Soc. Rev.* **2008**, *37*, 812-826.

37. Li, X.; Sayah, N.; Jackson, W. M., Laser Measurements of the Effects of Vibrational Energy on the Reactions of Cn. *J. Chem. Phys.* **1984**, *81*, 833-840.

38. Li, X.; Sayah, N.; Jackson, W. M., A Large Vibrational Enhancement in the Reaction of Cn (V '= 1, 2)+ No. *J. Chem. Phys.* **1985**, *83*, 616-622.

39. Klippenstein, S. J.; Yang, D.; Yu, T.; Kristyan, S.; Lin, M.; Robertson, S., A Theoretical and Experimental Study of the Cn+ No Association Reaction. *J. Phys. Chem. A* **1998**, *102*, 6973-6980.

40. Qian, C.; Noble, M.; Nadler, I.; Reisler, H.; Wittig, C., Ncno→ Cn+ No: Complete No (E, V, R) and Cn (V, R) Nascent Population Distributions from Well-Characterized Monoenergetic Unimolecular Reactions. *J. Chem. Phys.* **1985**, *83*, 5573-5580.

41. Nadler, I.; Noble, M.; Reisler, H.; Wittig, C., The Monoenergetic Vibrational Predissociation of Expansion Cooled Ncno: Nascent Cn (V, R) Distributions at Excess Energies 0–5000 Cm−. *J. Chem. Phys.* **1985**, *82*, 2608-2619.

42. Ruscic, B.; Pinzon, R. E.; Morton, M. L.; von Laszevski, G.; Bittner, S. J.; Nijsure, S. G.; Amin, K. A.; Minkoff, M.; Wagner, A. F., Introduction to Active Thermochemical Tables: Several "Key" Enthalpies of Formation Revisited. *J. Phys. Chem. A* **2004**, *108*, 9979-9997.

43. Abeysekera, C.; Joalland, B.; Shi, Y.; Kamasah, A.; Oldham, J. M.; Suits, A. G., Note: A Short-Pulse High-Intensity Molecular Beam Valve Based on a Piezoelectric Stack Actuator. *Rev. Sci. Instrum.* **2014**, *85*, 116107.

44. Brooke, J. S.; Ram, R. S.; Western, C. M.; Li, G.; Schwenke, D. W.; Bernath, P. F., Einstein a Coefficients and Oscillator Strengths for the a 2π-X 2σ+(Red) and B2σ+-X2σ+(Violet) Systems and Rovibrational Transitions in the X 2σ+ State of Cn. *Astrophys. J. Suppl. S.* **2014**, *210*, 23.

45. Fisher, W.; Eng, R.; Carrington, T.; Dugan, C.; Filseth, S.; Sadowski, C., Photodissociation of Brcn and Icn in the a Continuum: Vibrational and Rotational Distributions of Cn (X 2σ+). *Chem. Phys.* **1984**, *89*, 457-471.

46. Nadler, I.; Reisler, H.; Wittig, C., Energy Disposal in the Laser Photodissociation of Icn and Brcn at 300 K and in a Free Jet Expansion. *Chem. Phys. Lett.* **1984**, *103*, 451-457.

47. Hay, S.; Shokoohi, F.; Callister, S.; Wittig, C., Collisional Metastability of High Rotational States of Cn (X2σ+,= 0). *Chem. Phys. Lett.* **1985**, *118*, 6-11.

48. O'Halloran, M. A.; Joswig, H.; Zare, R. N., Alignment of Cn from 248 Nm Photolysis of Icn: A New Model of the ã Continuum Dissociation Dynamics. *J. Chem. Phys.* **1987**, *87*, 303-313.

49. Russell, J. A.; McLaren, I. A.; Jackson, W. M.; Halpern, J. B., Photolysis of Cyanogen Bromide between 193 and 266 Nm. *J. Phys. Chem.* **1987**, *91*, 3248-3253.

50. Huang, C.; Li, W.; Silva, R.; Suits, A. G., Dc Slice Ion Imaging of the Ultraviolet Photodissociation of Brcn. *Chem. Phys. Lett.* **2006**, *426*, 242-247.

51. Sabety-Dzvonik, M.; Cody, R., On Disequilibrated Rotational Distributions of Cn (X) Produced in the Photolysis of Clcn. *J. Chem. Phys.* **1976**, *64*, 4794-4796.

52. Heaven, M.; Miller, T. A.; Bondybey, V., Production and Characterization of Temperature-Controlled Free Radicals in a Free Jet Expansion. *Chem. Phys. Lett.* **1981**, *84*, 1-5.

53. Forthomme, D.; Hause, M. L.; Yu, H.-G.; Dagdigian, P. J.; Sears, T. J.; Hall, G. E., Doppler-Resolved Kinetics of Saturation Recovery. *J. Phys. Chem. A* **2015**, *119*, 7439-7450.

54. Hickson, K.; Sadowski, C.; Smith, I., Rate Coefficients for Removal of Cn ($X^2\sigma^+$ N= 2) from Selected Rotational Levels Ni= 0 to 57 in Collisions with $N_2$ and $C_2H_2$. *Chem. Phys. Lett.* **2003**, *372*, 443-450.

55. Wright, S. A.; Dagdigian, P. J., Investigation of the Effect of Reagent Cn Rotational Excitation on the Dynamics of the Cn+ O2 Reaction. *J. Chem. Phys.* **1995**, *103*, 6479-6489.

56. Alexander, M. H.; Hall, G. E.; Dagdigian, P. J., The Approach to Equilibrium: Detailed Balance and the Master Equation. *J. Chem. Educ.* **2011**, *88*, 1538-1543.

57. Herbert, L.; Smith, I. W.; Spencer-smith, R. D., Rate Constants for the Elementary Reactions between Cn Radicals and Ch4, C2h6, C2h4, C3h6, and C2h2 in the Range: 295⩽ T/K⩽ 700. *Int. J. Chem. Kinet.* **1992**, *24*, 791-802.

58. Lam, L.; Dugan, C.; Sadowski, C., The Gas Phase Reactions of Cn and No. *J. Chem. Phys.* **1978**, *69*, 2877-2881.

59. North, S. W.; Fei, R.; Sears, T. J.; Hall, G. E., Cn Radical Reaction Rate Measurements by Time-Resolved Fm Spectroscopy. *Int. J. Chem. Kinet.* **1997**, *29*, 127-129.

60. He, G.; Tokue, I.; Macdonald, R. G., Thermal Rate Constant for Cn+ H2/D2→ Hcn/Dcn+ H/D Reaction from T= 293 to 380 K. *J. Phys. Chem. A* **1998**, *102*, 4585-4591.

61. North, S. W.; Marr, A. J.; Furlan, A.; Hall, G. E., Nonintuitive Asymmetry in the Three-Body Photodissociation of Ch3cocn. *J. Phys. Chem. A* **1997**, *101*, 9224-9232.

62. Alagappan, A.; Costen, M. L.; McKendrick, K. G., Frequency Modulated Spectroscopy as a Probe of Molecular Collision Dynamics. *Spectrochim. Acta Part A Mol. Biomol. Spectrosc.* **2006**, *63*, 910-922.

63. Smith, I. W., The Reaction between Cn and 02: A Prototype Radical-Radical Reaction? In *The Chemical Dynamics and Kinetics of Small Radicals: Part 1*, 1995; pp 214-249.

64. Clary, D., Rates of Chemical Reactions Dominated by Long-Range Intermolecular Forces. *Mol. Phys.* **1984**, *53*, 3-21.

65. Reznickova, J. G.; Hippler, H.; Striebel, F.; Tevzadze, L., A Saturated Lif Study on the High Pressure Limiting Rate Constant of the Reaction Cn+ No+ M→ Ncno+ M between 200 and 600 K. *Z. Phys. Chem.* **2000**, *214*, 1115.

For Table of Contents Only